inorganics

MDPI

Review

Magnetostructural D-Correlations and Their Impact on Single-Molecule Magnetism

Ján Titiš [1,*], Cyril Rajnák [1] and Roman Boča [2]

[1] Department of Chemistry, FPV, University of SS Cyril and Methodius, 91701 Trnava, Slovakia; cyril.rajnak@ucm.sk
[2] Faculty of Health Sciences, University of SS Cyril and Methodius, 91701 Trnava, Slovakia; roman.boca@ucm.sk
* Correspondence: jan.titis@ucm.sk

Abstract: Functional dependence of the axial zero-field splitting parameter D with respect to a properly chosen geometrical parameter (D_{str}) in metal complexes is termed the magnetostructural D-correlation. In mononuclear hexacoordinate Ni(II) complexes with the ground electronic term $^3B_{1g}$ ($^3A_{2g}$ in the regular octahedron), it proceeds along two intercepting straight lines, allowing for predicting the sign and magnitude of the D-parameter by knowing the X-ray structure alone; D_{str} is constructed from the metal–ligand bond lengths. In hexacoordinate Co(II) complexes, it is applicable only in the segment of the compressed bipyramid where the ground electronic term $^4B_{1g}$ is orbitally non-degenerate so that the spin Hamiltonian formalism holds true. The D vs. D_{str} correlation is strongly non-linear, and it is represented by a set of decreasing exponentials. In tetracoordinate Co(II) complexes, on the contrary, the angular distortion from the regular tetrahedron is crucial so that the appropriate structural parameter D_{str} is constructed of bond angles. The most complex case is represented by pentacoordinated Co(II) systems, for which it is not yet possible to define a statistically significant correlation. All of these empirical correlations originate in the electronic structure of metal complexes that can be modelled using generalized crystal-field theory. As the barrier to spin reversal in single-molecule magnets is proportional to the D-value, for rational tuning and/or prediction of the single-molecule magnetic behaviour, knowledge/prediction of the D-parameter is beneficial. In this review, we present the statistical processing of an extensive set of structural and magnetic data on Co(II) and Ni(II) complexes, which were published over the past 15 years. Magnetostructural D-correlations defined for this data set are reviewed in detail.

Keywords: zero-field splitting; magnetostructural correlations; Ni(II) complexes; Co(II) complexes; single-molecule magnets

check for updates

Citation: Titiš, J.; Rajnák, C.; Boča, R. Magnetostructural D-Correlations and Their Impact on Single-Molecule Magnetism. *Inorganics* **2023**, *11*, 452. https://doi.org/10.3390/inorganics11120452

Academic Editor: Marius Andruh

Received: 24 September 2023
Revised: 31 October 2023
Accepted: 15 November 2023
Published: 23 November 2023

Copyright: © 2023 by the authors. Licensee MDPI, Basel, Switzerland. This article is an open access article distributed under the terms and conditions of the Creative Commons Attribution (CC BY) license (https://creativecommons.org/licenses/by/4.0/).

1. Introduction

Though a dodecanuclear plaquette-type complex, $[Mn^{III}_8Mn^{IV}_4O_{12}(ac)_{16}(H_2O)_4]\cdot 2Hac\cdot 4H_2O$, abbr. Mn12ac, was synthesized in 1980, its unusual magnetic properties were reported in 1991, and it was later termed a new class of magnetic materials—single-molecule magnets [1–12]. These systems show quantum effects, of which the most important is a slow magnetic relaxation. Slow means that the extrapolated relaxation time (time extrapolated to infinity temperature) is typically of the order $\tau_0 \sim 10^{-6}$–10^{-8} s, in contrast to spin glasses, where $\tau_0 < 10^{-20}$ s [13]. At a low enough temperature, the system retains its magnetization for a long enough time to find potential applications in recording techniques. Over the course of time, a plethora of 3d-metal complexes were identified as single-molecule magnets; for instance systems of different nuclearity cover Mn2, Mn3, Mn4, Mn6, Mn7, Mn8, Mn9, Mn10, Mn12, Mn16, Mn18, Mn21, Mn22, Mn25, Mn26, Mn30, Mn84, Fe4, Fe8, Fe9, Fe10, Fe11, Fe19, Co4, Co6, Ni4, Ni8, Ni12, Ni21, MnCu, V4, MnMo6, Mn2Cr, Mn2Fe, Mn2Ni2, Ni3Cr, Mn4Re4, Cu6Fe8, Co9W6, Co9Mo6, Mn8Fe4, etc. [14–29]. It can be

concluded that high nuclearity is not an ultimate demand for single-molecule magnetic behaviour since many mononuclear complexes of Cr(III), Mn(III), Mn(II), Fe(III), Fe(II), Fe(I), Co(II), and Ni(II) possessing the spin S = 1 through 5/2 also show slow magnetic relaxation [30–32]. Moreover, some S = 1/2 spin systems, such as V(IV), low-spin Mn(IV), low-spin Co(II), low-spin Ni(III), Ni(I), and Cu(II), exhibit slow magnetic relaxation as well [33–36]. Slow magnetic relaxation and single-molecule magnetism were identified among 4f-complexes (mononuclear and polynuclear) as well as heterometallic 4f-3d complexes; for instance, Tb1, Dy1, TbCu, Dy2, Dy4, Dy6Mn6, Dy4Mn11, and many others were classified as single-molecule magnets [14].

In contrast to classical magnetic materials (like ferrites that are widely used in daily recording techniques and many useful tools), a single-molecule magnet retains its magnetization due to magnetic anisotropy. The magnetic anisotropy in single crystals is defined as the non-isotropic magnetization tensor having at least two different main axis components, or the non-isotropic susceptibility tensor. In molecules, the spin–spin interaction tensor, when rotated to its main axes, possesses the diagonal elements

$$\hat{H}^{\mathrm{ss}} = \hbar^{-2}(D_{xx}\hat{S}_x^2 + D_{yy}\hat{S}_y^2 + D_{zz}\hat{S}_z^2) \quad (1)$$

that define two eccentricity parameters:

(a) The axial zero-field splitting (ZFS) parameter D

$$D = (-D_{xx} - D_{yy} + 2D_{zz})/2 \rightarrow (3/2)D_{zz} \quad (2)$$

(b) The (ortho)rhombic ZFS parameter E

$$E = (D_{xx} - D_{yy})/2 \quad (3)$$

These two parameters modify (split) the ground state energy levels in the absence of the magnetic field, and they are responsible for magnetic anisotropy. Magnetic anisotropy manifests itself in the way that, with an increasing magnetic field, the magnetization components as well as the magnetic susceptibility (Cartesian) components develop differently.

Using the ZFS parameters, the spin–spin interaction can be rewritten to the form

$$\hat{H}^{\mathrm{ss}} = \hbar^{-2}[D(\hat{S}_z^2 - \hat{S}^2/3) + E(\hat{S}_x^2 - \hat{S}_y^2)] \quad (4)$$

and usually, a constraint $|D| \geq 3E \geq 0$ is maintained. For a uniaxial system (like D_{4h} or C_{4v}), the effective spin-Hamiltonian collapses to

$$\hat{H}^{\mathrm{aniso}} = \hbar^{-2}D_S\hat{S}_z^2 \quad (5)$$

giving rise to energy levels depending upon the magnetic quantum number M

$$\varepsilon = D_S M^2 \quad (6)$$

(In these formulae, it is emphasized that we are working in the strong exchange limit for polynuclear systems, so that the D-parameter depends on the (good) total molecular spin quantum number S; hence, D_S.) When $D_S > 0$ (easy-plane anisotropy), a model of a particle in the potential box is appropriate: a fast relaxation from the state $M = -S$ to $M = 0$ (or $M = \pm 1/2$) proceeds, and the magnetic record disappears. On the contrary, when $D_S < 0$ (easy-axis anisotropy) a model of a particle in the double potential is applicable; the two minima are separated by a barrier to spin reversal $\Delta E = |D_S|S^2$ (or $\Delta E = |D_S|S^2 - |D_S|/4$ for the half-integral spin) and thermal activation mechanism of the relaxation, or tunnelling mechanism, apply. Based on this reasoning, a deep knowledge about the D_S-parameter is a key factor for a rational synthesis of single-molecule magnets with aimed properties. The rhombic ZFS parameter E_S is also in play through the term $E_S(\hat{S}_x^2 - \hat{S}_y^2)$, and it causes a further modification in the energy levels and consequently, the single-molecule magnetic behaviour.

2. Spin-Hamiltonian Formalism

The spin-Hamiltonian (SH) formalism is applicable when the ground electronic term is orbitally non-degenerate (e.g., $^3A_{2g}$, $^4B_{1g}$). In this model, the electronic wave function is substituted by spin-only kets $|S, M_S\rangle$. This very restricted basis set is under the action of operators covered by three leading terms: the spin Zeeman term, the orbital Zeeman term, and the spin–orbit interaction term

$$\hat{H}' = \hbar^{-1}\mu_B g_e(\vec{S}\cdot\vec{B}) + \hbar^{-1}\mu_B(\vec{L}\cdot\vec{B}) + \hbar^{-2}\lambda(\vec{L}\cdot\vec{S}) \quad (7)$$

where g_e is the spin-only magnetogyric factor and $\lambda = \pm\xi/2S$ is the spin–orbit splitting parameter within the ground electronic term dependent upon the spin–orbit coupling constant ξ (the minus sign applies for the configurations d^n more than half-full). Then, the second-order perturbation theory yields the contribution [37]

$$\hat{H}^S = \hbar^{-2}(\vec{S}\cdot\overline{\overline{D}}\cdot\vec{S}) + \hbar^{-1}\mu_B(\vec{B}\cdot\overline{\overline{g}}\cdot\vec{S}) + (\vec{B}\cdot\overline{\overline{\kappa}}\cdot\vec{B}) \quad (8)$$

To this end, three magnetic tensors contribute:

- The D-tensor (tensor of the spin–spin interaction)

$$D_{ab} = \lambda^2\Lambda_{ab}\ [\text{energy}] \quad (9)$$

- The g-tensor (tensor of the magnetogyric ratio)

$$g_{ab} = g_e\delta_{ab} + 2\lambda\Lambda_{ab}\ [\text{dimensionless}] \quad (10)$$

- The κ-tensor (tensor of the temperature-independent paramagnetism)

$$\kappa_{ab} = \mu_B^2\Lambda_{ab}\left[\text{energy}\times\text{induction}^{-2}\right] \quad (11)$$

All of them are constituted of the Λ-tensor (tensor of the angular momentum unquenching)

$$\Lambda_{ab} = -\hbar^{-2}\sum_{K\neq 0}\frac{\langle 0|\hat{L}_a|K\rangle\langle K|\hat{L}_b|0\rangle}{E_K - E_0}\left[\text{energy}^{-1}\right] \quad (12)$$

where the summation runs over all excited states (electronic terms). The scalar product of the vectors and tensors can be developed as follows

$$\hat{H}^S = \sum_a^{x,y,z}\sum_b^{x,y,z}\left\{\hbar^{-2}\lambda^2\Lambda_{ab}\hat{S}_a\hat{S}_b + \hbar^{-1}\mu_B B_a(g_e\delta_{ab} + 2\lambda\Lambda_{ab})\hat{S}_b + \mu_B^2\Lambda_{ab}B_aB_b\right\} \quad (13)$$

In the zero magnetic field, we arrive at the Formulae (1)–(4), which are widely used in analysing the magnetic data (susceptibility and magnetization) as well as the spectroscopic data such as Electron–Spin–Resonance (ESR) or Far-Infra-Red (Far-IR) spectra referring to electronic transitions.

For degenerate ground electronic terms of the T-type, the above formalism is inappropriate, and one is left to pass beyond the spin-Hamiltonian formalism. In the early stages, it was covered by Griffith and Figgis' theory, respectively, dealing with the ground $T_{1(g)}$ or $T_{2(g)}$ terms, eventually under symmetry lowering and configuration interaction [38,39]. A more complete approach that involves all members of the d^n-electron configuration was outlined by the König–Kremer theory [40–42].

3. Electronic Structure of 3d-Complexes

An almost complete description of the energy levels in metal d- or f-complexes can be obtained by considering five operators acting to the basis set of free-atom terms $|l^n v L S M_L M_S\rangle$ with the seniority number v:

(a) The interelectron repulsion

$$H_{IJ}^{\mathrm{ee}} = \left\langle l^n vLSM_L M_S \middle| \hat{V}^{\mathrm{ee}} \middle| l^n v'L'S'M_L{}'M_S{}' \right\rangle = \delta_{M_L,M_L{}'}\delta_{M_S,M_S{}'}\delta_{L,L'}\delta_{S,S'} \left\langle l^n vLS \middle\| \sum_{i=1}^{n}\sum_{j>i}^{n}\sum_{k=0,2,4}^{2l} F_{ll}^{k} \sum_{q=-k}^{+k} (-1)^q \hat{C}_{-q}^{k}(i)\hat{C}_{q}^{k}(j) \middle\| l^n v'L'S' \right\rangle \tag{14}$$

(b) The crystal-field potential

$$H_{IJ}^{\mathrm{cf}} = \left\langle l^n vLSM_L M_S \middle| \hat{V}^{\mathrm{cf}} \middle| l^n v'L'S'M'_L M'_S \right\rangle = \delta_{S,S'}\delta_{M_S,M_S{}'} \left\langle l^n vLSM_L M_S \middle| \sum_{i=1}^{n}\sum_{K=1}^{N} z_K \sum_{k=0,2,4}^{2l} F_k(R_K) \sum_{q=-k}^{+k} (-1)^q \hat{C}_{-q}^{k}(K)\hat{C}_{q}^{k}(i) \middle| l^n v'L'S'M_L{}'M_S{}' \right\rangle \tag{15}$$

(c) The spin–orbit interaction

$$\begin{aligned} H_{IJ}^{\mathrm{so}} &= \left\langle l^n vLSM_L M_S \middle| \hat{V}^{\mathrm{so}} \middle| l^n v'L'S'M_L{}'M_S{}' \right\rangle \\ &= \left\langle l^n vLSM_L M_S \middle| \hbar^{-2} \sum_{i=1}^{n} \xi_i (\vec{l}_i \cdot \vec{s}_i) \middle| l^n v'L'S'M_L{}'M_S{}' \right\rangle \end{aligned} \tag{16}$$

(d) The orbital Zeeman term

$$\begin{aligned} H_{IJ}^{\mathrm{lB}} &= \left\langle l^n vLSM_L M_S \middle| \hat{V}^{\mathrm{lB}} \middle| l^n v'L'S'M_L{}'M_S{}' \right\rangle \\ &= \delta_{v,v'}\delta_{L,L'}\delta_{S,S'}\delta_{M_S,M_S{}'} \left\langle l^n vLSM_L M_S \middle| \hbar^{-1}\mu_{\mathrm{B}}\kappa(\vec{B}\cdot\vec{L}) \middle| l^n v'L'S'M_L{}'M_S{}' \right\rangle \end{aligned} \tag{17}$$

(e) The spin Zeeman term

$$\begin{aligned} H_{IJ}^{\mathrm{sB}} &= \left\langle l^n vLSM_L M_S \middle| \hat{V}^{\mathrm{sB}} \middle| l^n v'L'S'M_L{}'M_S{}' \right\rangle \\ &= \delta_{v,v'}\delta_{L,L'}\delta_{S,S'}\delta_{M_L,M_L{}'} \left\langle l^n vLSM_L M_S \middle| \hbar^{-1}\mu_{\mathrm{B}} g_{\mathrm{e}} (\vec{B}\cdot\vec{S}) \middle| l^n v'L'S'M_L{}'M_S{}' \right\rangle \end{aligned} \tag{18}$$

Here, the Racah operator (rationalized spherical harmonics) $\hat{C}_q^k(i) = (4\pi/2k+1)^{1/2}\, Y_q^k(i)$ occurs, where k—rank and q—component. The parameter

$$F_k(R_K) = \left(e^2/4\pi\varepsilon_0\right)\left\langle r_{>}^{-(k+1)} \cdot r_{<}^{k} \right\rangle \approx \left(e^2/4\pi\varepsilon_0\right) R_K^{-(k+1)} \cdot \left\langle r^k \right\rangle \tag{19}$$

refers to the crystal field strength of the K-th ligand (R_K defines the distance of the ligand from the central atom); $F_{ll}^k = \left(e^2/4\pi\varepsilon_0\right)\left\langle r_{>}^{-(k+1)} \cdot r_{<}^{k} \right\rangle$ are Slater–Condon parameters of rank k. The orbital Zeeman term includes κ—an orbital reduction factor. The advantage of this approach is that all matrix elements can be expressed using closed formulae [37]. By selecting a certain combination of operators/matrix elements, several cases can be mapped:

(i) By diagonalizing the matrix

$$H_{IJ} = H_{IJ}^{\mathrm{ee}} + H_{IJ}^{\mathrm{cf}} \tag{20}$$

the resulting eigenvalues refer to the energies of crystal field terms. No constrain to the crystal field strength is needed (weak field, strong field, intermediate field) since the variation principle is applied. The resulting eigenvectors $|l^n(vL)SM_S\Gamma\gamma a\rangle$ can be probed for symmetry operations of the respective point group of symmetry, allowing for a classification according to the irreducible representations $\Gamma\gamma$ (like A_{2g}, T_{1g}, and T_{2g} for the group O_h of the d^8 system, in Mulliken notation).

(ii) By diagonalizing the matrix

$$H_{IJ} = H_{IJ}^{\mathrm{ee}} + H_{IJ}^{\mathrm{cf}} + H_{IJ}^{\mathrm{so}} \tag{21}$$

one obtains the crystal field multiplets. The eigenvectors $|l^n(vLS)J\Gamma'\gamma' b\rangle$, when probed for symmetry operations of the respective double group, yield an assignment of the Bethe symbols (Γ_1 through Γ_8 for the O′ double group) to the energy levels.

(iii) By diagonalizing the matrix

$$H_{IJ} = H_{IJ}^{\mathrm{ee}} + H_{IJ}^{\mathrm{cf}} + H_{IJ}^{\mathrm{so}} + H_{IJ}^{\mathrm{lB}}(B) + H_{IJ}^{\mathrm{sB}}(B) \quad (22)$$

the Zeeman levels dependent on the magnetic field are obtained. They enter the partition function $Z(B,T)$, from which the magnetization components $M_a(B,T)$, the susceptibility components $\chi_{ab}(B,T)$, and eventually, the heat capacity $c_V(B,T)$ can be obtained with the apparatus of statistical thermodynamics [37].

The above matrices, in general, are complex-Hermitian, so the programming requires complex*16 arithmetic. The size of the basis set for d^5 through d^9 systems is 256, 210, 120, 45, and 10 members, respectively. In this approach, the configuration interaction is naturally involved, and it is termed the Generalized Crystal-Field Theory (GCFT).

4. Zero-Field Splitting Parameters

The application of the spin-Hamiltonian formalism offers modelling of the energy levels, magnetization, and magnetic susceptibility depending upon the spin quantum numbers S = 1, 3/2, 2, and 5/2. The corresponding spin matrices have dimensions of 3, 4, 5, and 6 in the basis set of spin kets $|S, M_S\rangle$. The members of the spin multiplets in the zero field are separated by amount D, 2D, (D, 3D), and (2D, 4D), respectively, as shown in Figure 1.

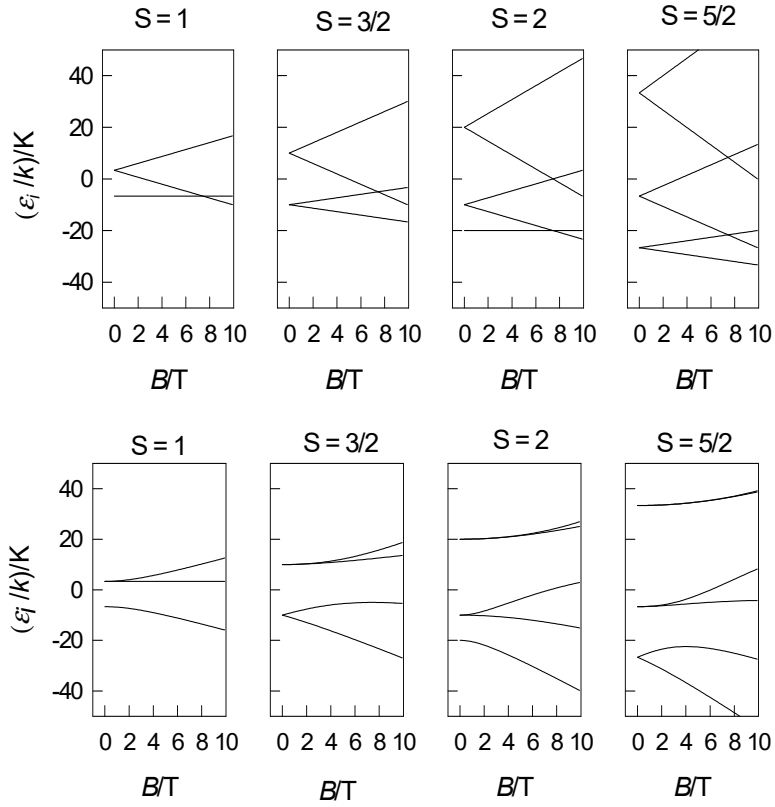


Figure 1. Energy levels modelled with the spin-Hamiltonian formalism, D/k = 10 K; parallel direction (z)-(**upper panel**); perpendicular direction (x)-(**bottom panel**).

In general, the spin Zeeman term depends on the polar coordinates (ϑ, φ) as follows

$$\hat{H}_{kl,m}^{Z} = \mu_{\mathrm{B}} B_m (g_x \sin\vartheta_k \cos\varphi_l \hat{S}_x + g_y \sin\vartheta_k \sin\varphi_l \hat{S}_y + g_z \cos\vartheta_k \hat{S}_z)\hbar^{-1} \quad (23)$$

where (k, l) refer to grids distributed uniformly over a sphere. In this way, the magnetization can be visualized with a 3D diagram, as shown in Figure 2. It must be noted that when $|D| < 3E$, a renumbering of the Cartesian axes results in the usual constraint $|D| > 3E$. In a very high field (50 T), the system becomes isotropic, and its 3D magnetization refers to a sphere.

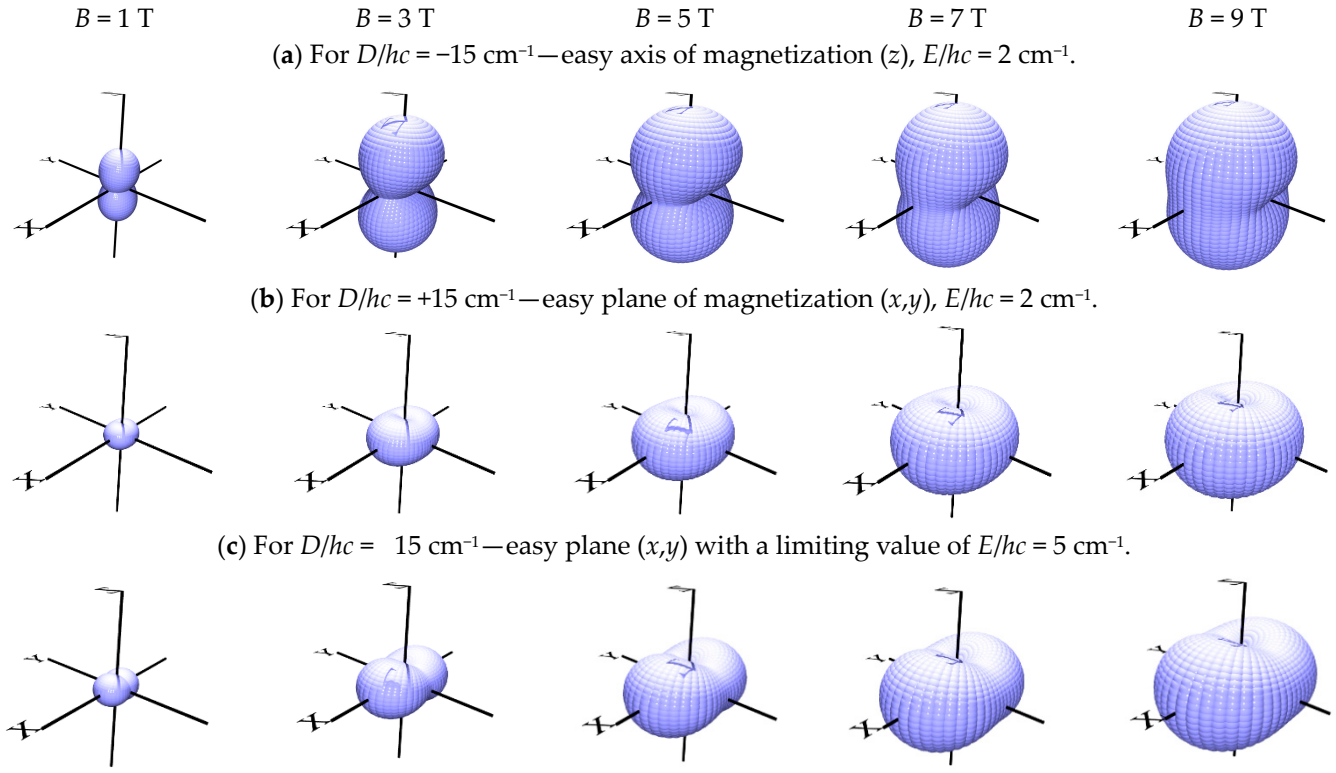


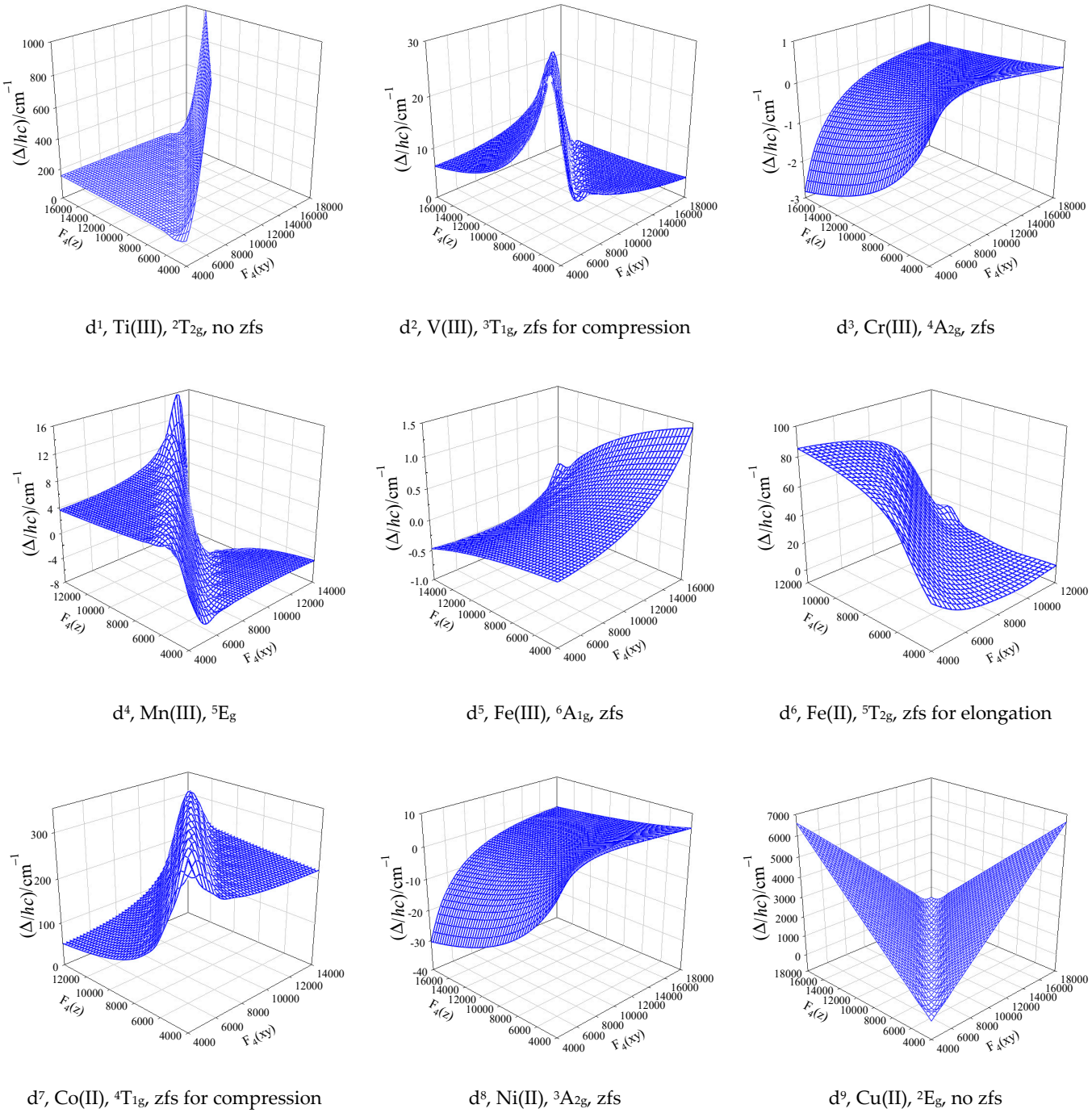
Figure 2. Three-dimensional view of the magnetization $M(D,E)$ for different applied fields, $S = 1$.

At the higher level of the theory (GCFT), when all members of the d^n configuration are considered, the D and E values are not rigorously defined. Figure 3 brings the modelling of the lowest energy gap among crystal field multiplets beyond the SH formalism using GCFT for a wide range of crystal field strengths, which is briefly discussed below.

The octahedral d^3 and d^8 systems are fortunate cases since the ground electronic term is nondegenerate ($^4A_{2g}$, $^3A_{2g}$), and it stays nondegenerate for the whole array of compressed and elongated tetragonal bipyramids ($^4B_{1g}$, $^3B_{1g}$). For Ni(II) complexes ($S = 1$), the lowest crystal field multiplets, labelled in the D'_4 double group by Bethe (Mulliken) symbols $\Gamma_4(B_2)$ and $\Gamma_5(E_1)$, are separated by the energy gap $\Delta = \varepsilon(\Gamma_5) - \varepsilon(\Gamma_4)$; this value adopts role of the D-parameter (the Γ_5 level is doubly degenerate in the zero field). $D > 0$ applies for an elongated tetragonal bipyramid, and $D < 0$ holds true for the compressed bipyramid. For the octahedral geometry, the energy gap collapses to zero. The range of D-values for Cr(III) is by one order of magnitude lower relative to Ni(II); this is a consequence of a much lower spin–orbit splitting parameter $\lambda/hc = 92$ vs. 315 cm^{-1} ($D \sim \lambda^2$).

The octahedral d^7 system possesses the ground term $^4T_{1g}$, which is orbitally triply degenerate. Upon distortion to a compressed tetragonal bipyramid, it is split into $\{^4A_{2g}, ^4E_g\}$ terms; upon distortion to an elongated bipyramid, the splitting is opposite $\{^4E_g, ^4A_{2g}\}$. The spin–orbit coupling causes a further splitting into six Kramer doublets: $1\Gamma_6$, $1\Gamma_7$, $2\Gamma_6$, $3\Gamma_6$, $2\Gamma_7$, and $3\Gamma_7$ for the compression and $1\Gamma_6$, $2\Gamma_6$, $1\Gamma_7$, $2\Gamma_7$, $3\Gamma_6$, and $3\Gamma_7$ for the elongation. This means that only the first case is consistent with the SH formalism. Moreover, the crystal field asymmetry should be large (much stronger axial crystal field $F_4(z)$); in such a case, always $\Delta = 2D > 0$, and it is very high (typically 200 cm^{-1}).

The counter parting d^2 system with the ground state $^3T_{1g}$ resembles tetragonal splitting into $\{^3A_{2g}, ^3E_g\}$ upon compression, and the spin–orbit coupling splits the ground term into $\Gamma_1(A_1)$ and $\Gamma_5(E_1)$ multiplets. In this case, $\Delta = D > 0$ holds true. For the elongated bipyramid, the six-membered multiplet manifold is $\Gamma_3(B_1)$, $\Gamma_4(B_2)$, $\Gamma_5(E_1)$, $\Gamma_1(A_1)$, and $\Gamma_2(A_2)$, and it has no relationship with the SH approach.



d¹, Ti(III), $^{2}T_{2g}$, no zfs

d², V(III), $^{3}T_{1g}$, zfs for compression

d³, Cr(III), $^{4}A_{2g}$, zfs

d⁴, Mn(III), $^{5}E_{g}$

d⁵, Fe(III), $^{6}A_{1g}$, zfs

d⁶, Fe(II), $^{5}T_{2g}$, zfs for elongation

d⁷, Co(II), $^{4}T_{1g}$, zfs for compression

d⁸, Ni(II), $^{3}A_{2g}$, zfs

d⁹, Cu(II), $^{2}E_{g}$, no zfs

Figure 3. Lowest energy gap calculated with the GCFT over a wide range of crystal field strengths between a compressed and elongated tetragonal bipyramid (D_{4h}) for the electron configurations d^1 through d^9 (the given terms refer to O_h symmetry). The *D*-parameter results from the splitting of a non-degenerate ground electronic term by the spin–orbit interaction.

For Mn(III) systems (d^4, $S = 2$), the situation is more complex. The spin-Hamiltonian (SH) formalism predicts that for $D > 0$ (compressed tetragonal bipyramid), the ground state $|S, M_S\rangle$ is a singlet $|2, 0\rangle$.The first excited Kramer doublet $|2, \pm1\rangle$ is a *D*-value higher, and the second excited Kramer doublet $|2, \pm2\rangle$ lies a $4D$ amount above the ground state. The GCFT is consistent with the SH formalism only for the first three multiplets Γ_1 and Γ_5 (doubly degenerate). The remaining two excited states, Γ_3 and Γ_4, are not exactly degenerate (they do not form a Kramer doublet), but they are split in the zero field by

0.2 cm^{-1}. (The calculated energy levels are, for instance: $\Gamma_1(A_1) \times 1$ at 0; $\Gamma_5(E_1) \times 2$ at 5.1 cm^{-1} and $\Gamma_3(B_1) \times 1$ at 19.8 cm^{-1}; $\Gamma_4(B_2) \times 1$ at 20.0 cm^{-1}. Thus, for D = 5.1 cm^{-1} is $4D$ = 20.4 cm^{-1}, but the Γ_4 level is 0.4 cm^{-1} lower.) This demonstrates that we cannot rely on the spin-Hamiltonian formalism in all cases.

The d^6 system, similar to high-spin Fe(II), again is a complex task. In the octahedral geometry, the ground term is orbitally triply degenerate, $^5T_{2g}$. Upon tetragonal elongation, it is split into $\{^5B_{2g}, {}^5E_g\}$ terms, and five members of the ground term $^5B_{2g}$ are further split by the spin–orbit interaction into multiplets Γ_4, Γ_5, Γ_1, and Γ_2. Then, the SH formalism is approximately valid (the Γ_1, Γ_2 pair is quasi-degenerate and separated from the ground Γ_4 by ca. $4D$); the D-value is moderate: D/hc~10 cm^{-1}. Upon tetragonal compression, the 10-membered manifold of the ^5E_g term is split in a way having no relationship to the SH formalism, so that the D-parameter is undefined.

The electronic structure of tetrahedral d^n systems matches complementary octahedral systems d^{10-n}. For instance, tetrahedral Co(II)—d^7 possesses the ground state $^4A_2$, similar to octahedral Cr(III)—d^3. All GCFT calculations were carried out using our own software written in Fortran [37,43].

5. Magnetostructural J-Correlations

Before proceeding to the discussion of magnetostructural D-correlations, we briefly mention the original type of Correlation Analysis of structure–magnetism relations in transition metal complexes. Relationships between selected structural parameters and the magnetic properties of dinuclear (polynuclear) metal complexes were outlined by Hatfield [44,45], his co-workers, and followers. In [Cu^{II}-$(OH)_2$-Cu^{II}]-type complexes, the isotropic exchange constant J correlates with the bond angle α = Cu-O-Cu along a straight line with negative slope

$$J[cm^{-1}] = -74.53 \cdot \alpha[^\circ] + 7270, \; r = -0.99 \quad (24)$$

Involvement of more data with greater structural diversity along the superexchange path led to a differentiation according to the alkoxido- or phenoxido-class [46]. Analogous linear correlations were developed for [Cr^{III}-$(OH)_2$-Cr^{III}]- and [Mn^{IV}-$(O)_2$-Mn^{IV}]-type complexes [47–49].

According to Gorun and Lippard, the J-value correlates with the shortest Fe-O distance (abbr. P) along the superexchange path in [Fe^{III}-O-Fe^{III}]-type complexes [50,51]. The correlation was proposed along a decreasing exponential curve that is applicable only in the segment of negative J

$$-J[cm^{-1}] = (2.360 \times 10^{10}) \cdot \exp(-10.661 \, P[10^{-10} \text{ m}]), \; r = -0.97 \quad (25)$$

However, a linear correlation is also acceptable; hence

$$J[cm^{-1}] = 525.7 \cdot P[10^{-10} \text{ m}] - 1055, \; r = 0.96 \quad (26)$$

It must be critically said that any kind of magnetostructural relationship or correlation heavily depends upon the quality of structural and magnetic data. Another aspect is that almost all correlations are restricted to the linear relationships of the J-α or J-P types. Nowadays, modern statistical software packages (multivariate methods) are at our disposal. Correlation Analysis, Cluster Analysis, Principal Component Analysis, Factor Analysis, etc., can be applied to carefully filtered datasets. An approach similar to this appeared very recently [52].

6. Magnetostructural D-Correlations

It is obvious that the correlation D vs. P (a geometrical parameter) is derived from the electronic structure of complexes. The problem of electronic structure, as well as magnetic properties, is solved mainly at the level of quantum–chemical (first-principle) calculations [53–55]. The application of the partitioning technique and/or quasi-degenerate

perturbation theory yields the matrix elements of the effective Hamiltonian spanned by the spin manifold of the orbitally non-degenerate ground electronic state $|0SM\rangle$ as follows

$$\begin{array}{c}\left\langle 0SM\middle|\hat{H}_{\text{eff}}\middle|0SM'\right\rangle = E_0\delta_{MM'} + \left\langle 0SM\middle|\hat{H}_1\middle|0SM'\right\rangle \\ -\sum\limits_{bS''M''}\Delta_b^{-1}\left\langle 0SM\middle|\hat{H}_1\middle|bS''M''\right\rangle\cdot\left\langle bS''M''\middle|\hat{H}_1\middle|0SM'\right\rangle\end{array} \quad (27)$$

with the denominator defined by excitation energies

$$\Delta_b^{-1} = (E_b - E_0)^{-1},\ E_0 = \left\langle 0SM\middle|\hat{H}_0\middle|0SM\right\rangle \quad (28)$$

Then, the D-tensor components (m, n = x, y, z) arising from the spin–orbit interaction are obtained in the form

$$\begin{array}{c}D_{mn}^{(0)} = -\frac{1}{S^2}\sum\limits_{b(S_b=S)}\Delta_b^{-1}\left\langle 0SS\middle|\sum\limits_i \hat{h}_m^{(i)}\hat{s}_z^{(i)}\middle|bSS\right\rangle \\ \cdot\left\langle bSS\middle|\sum\limits_i \hat{h}_n^{(i)}\hat{s}_z^{(i)}\middle|0SS\right\rangle\end{array} \quad (29)$$

$$\begin{array}{c}D_{mn}^{(-1)} = -\frac{1}{S(2S-1)}\sum\limits_{b(S_b=S-1)}\Delta_b^{-1}\left\langle 0SS\middle|\sum\limits_i \hat{h}_m^{(i)}\hat{s}_{+1}^{(i)}\middle|b,S-1,S-1\right\rangle \\ \cdot\left\langle b,S-1,S-1\middle|\sum\limits_i \hat{h}_n^{(i)}\hat{s}_{-1}^{(i)}\middle|0SS\right\rangle\end{array} \quad (30)$$

$$\begin{array}{c}D_{mn}^{(+1)} = -\frac{1}{(S+1)(2S+1)}\sum\limits_{b(S_b=S+1)}\Delta_b^{-1}\left\langle 0SS\middle|\sum\limits_i \hat{h}_m^{(i)}\hat{s}_{-1}^{(i)}\middle|b,S+1,S+1\right\rangle \\ \cdot\left\langle b,S+1,S+1\middle|\sum\limits_i \hat{h}_n^{(i)}\hat{s}_{+1}^{(i)}\middle|0SS\right\rangle\end{array} \quad (31)$$

where the one-electron (i) orbital operator for the spin–orbit coupling is

$$\hat{h}_m^{(i)} = \sum_A \xi_A^{(i)}\hat{l}_{mA}^{(i)} \quad (32)$$

A comparison with the simple perturbation theory applied to the crystal field terms arising from the d-electrons of the central atom [56–58]

$$D_{mn}^{\text{CFT}} = -\frac{1}{4S^2}\sum_{K\neq 0}\frac{\langle 0|\hat{L}_m\xi|K\rangle\langle K|\hat{L}_n\xi|0\rangle\hbar^{-2}}{E_K - E_0} \quad (33)$$

shows that more contributions are in play. Quantum–chemical calculations show that the individual contributions to the D-parameter are different in size and sign, and a lot of terms approximately cancel. The dominating part arises from the spin–orbit coupling; however, the contributions from the spin–spin interaction also cannot be completely neglected in many cases [59].

A much more simplified approach is GCFT. By inspecting Figure 4, it is possible to transform the 3D graph $D = f(F_4(xy), F_4(z))$ into a 2D diagram $D = f(P)$. The crystal field poles can be expressed with the fourth electronic moment $< r^4 >$, common for the complex as follows

$$F_4(R_K) \approx \left(e^2/4\pi\varepsilon_0\right)R_K^{-5}\left\langle r^4\right\rangle \quad (34)$$

hence, the relationship

$$\left(e^2/4\pi\varepsilon_0\right)\left\langle r^4\right\rangle = F_4(z)R_z^5 = F_4(xy)R_{xy}^5 \quad (35)$$

holds true. This method enables relatively fast mapping of the structural dependence of the D-parameter for a wide range of distortions.

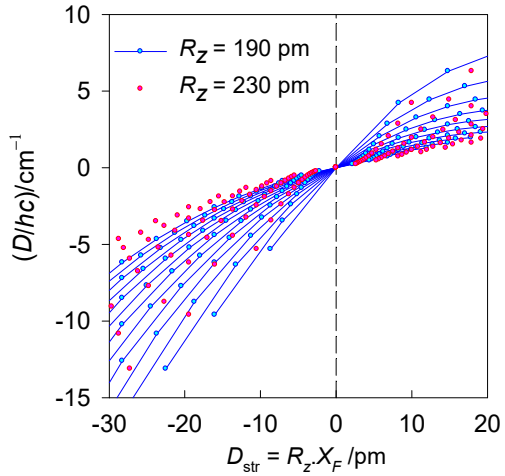


Figure 4. Calculated magnetic *D*-values (exact multiplet splitting with GCFT) for different equatorial-axial crystal field strengths vs. the transformed structural ordinate D_{str} for hexacoordinate Ni(II) complexes. Solid lines interpolate the points for common axial metal-ligand distance R_z = 190 pm. Red points bracket the second limiting case, R_z = 230 pm.

6.1. Hexacoordinate Ni(II) Complexes

Magneto-structural relationships for the nearly-octahedral Ni(II) complexes were mapped along a tetragonal distortion mode characterized by the difference between axial (R_z) and equatorial (R_{xy}) metal–ligand bond lengths. Thus, the structural *D*-parameter can be expressed by introducing the X_F function as follows

$$D_{\mathrm{str}} = R_z - R_{xy} = R_z \left[1 - \left(\frac{F_4(z)}{F_4(xy)} \right)^{1/5} \right] = R_z \cdot X_F \tag{36}$$

A modelling of the magnetic *D*-values (exact multiplet splitting) depending on the transformed structural ordinate is shown in Figure 4. The important message is that such dependence is generally non-linear; however, within the relevant experimental range, it follows a nearly linear relationship. In fact, the dependence—the correlation line of the magnetostructural D-correlation—is represented by a pair of nearly collinear straight lines intercepting at the octahedral geometry where *D* and D_{str} are zero. The calculations using GCFT were performed for the nephelauxetic ratio β = 1, and the orbital reduction factors $\kappa_z = \kappa_{xy}$ = 1; therefore, the results are tentative.

The magnetic data used hereafter were collected quite recently using the SQUID magnetometer. The magnetic susceptibility (χ) was taken at the applied field of B_{DC} = 0.1 T between *T* = 1.9 and 300 K. The magnetization data (*M*) were taken at *T* = 2.0 and 4.6 K, respectively, up to *B* = 5 or 7 T. Both datasets were fitted simultaneously using a numerical procedure that minimizes a joint functional $F = R(\chi) \cdot R(M)$. A collection of 25 datapoints (objects = complexes under study) is displayed in Figure 5 along with a common linear correlation *D* vs. D_{str}. This simple regression analysis was performed in SigmaPlot software [60] and clearly confirms the linear dependence in the given interval of D_{str} values. Based on the analysis of variance (ANOVA), one can conclude that the independent variable D_{str} can be used to predict the dependent variable *D* (large *F* and $P < 0.05$). A list of the compounds and numerical data is provided in the Supplementary Information [61,62]. The correlation predicts that with increasing structural tetragonality D_{str} (in the direction compressed tetragonal bipyramid–octahedron–elongated tetragonal bipyramid), the axial zero-field splitting parameter *D* increases.

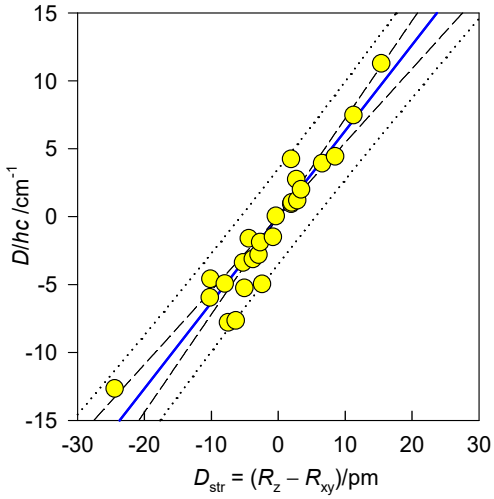


Figure 5. Magnetostructural D-correlation for hexacoordinate Ni(II) complexes, $D = a + b \cdot D_{\mathrm{str}}$ ($a = -0.31$, $b = 0.62$, $R^2 = 0.89$, ANOVA: $F = 206.12$, $P < 0.0001$). Confidence (dashed line) and prediction (dotted line) intervals are shown at the 95% probability level.

It must be mentioned that for the complexes with a heterogeneous coordination sphere, e.g., possessing $\{NiN_4O_2\}$ chromophore, the evaluation of the experimental value of D_{str} requires a correction taking into account the averaged bond lengths of the given donor atom. For instance

$$D_{\mathrm{str}} = \Delta_z - (\Delta_y + \Delta_x)/2 \tag{37}$$

where $\Delta_a = (R_a - \overline{R}_a)$ for $a = x$, y, and z is a shift relative to the mean distance $\overline{R}_a$ for a given bond. For the N- and O-donor ligands, these values were taken from complexes containing $[Ni(NH_3)_6]^{2+}$ and $[Ni(H_2O)_6]^{2+}$ units, respectively, $\overline{R}(\mathrm{Ni-N}) = 2.145$ and $\overline{R}(\mathrm{Ni-O}) = 2.055$ Å. For a more ionic bond, the value of $\overline{R}(\mathrm{Ni-NCS}) = 2.070$ Å was used.

Another piece of information is obtained from the multivariate data analysis, which we performed using the Statgraphics software [63]. Principal Component Analysis (PCA) transforms the set of original variables into their linear combinations (principal components), bearing the maximum variability in the data. Two components bear 94.7% of the variability in the present case. The biplot in Figure 6 shows how the individual variables are interrelated: the closest rays refer to a positive correlation, and the farthest rays refer to a negative correlation (anticorrelation). The graph proves that the g-factor asymmetry (gdif = $g_z - g_{xy}$) anticorrelates with the D-parameter, in agreement with the spin-Hamiltonian formula $D = -(\xi/2S)(g_z - g_{xy})/2$. On the other hand, it confirms the strong positive correlation between D and D_{str}. Classification of the individual points according to the clusters allows us to visualize the clusters' separation.

Factor Analysis (FA) constructs a small number of new variables—common factors that represent a large percentage of the variability in the original variables. Factor loadings may be obtained from either the sample covariance or sample correlation matrix. The initial loadings may be rotated (e.g., with varimax rotation). Two factors cover 96.5% of the variability in the original data (D_{str}, D, g_{xy}, and g_z) in the present case (Figure S1). Again, the strong correlation between parameters D and D_{str} is confirmed.

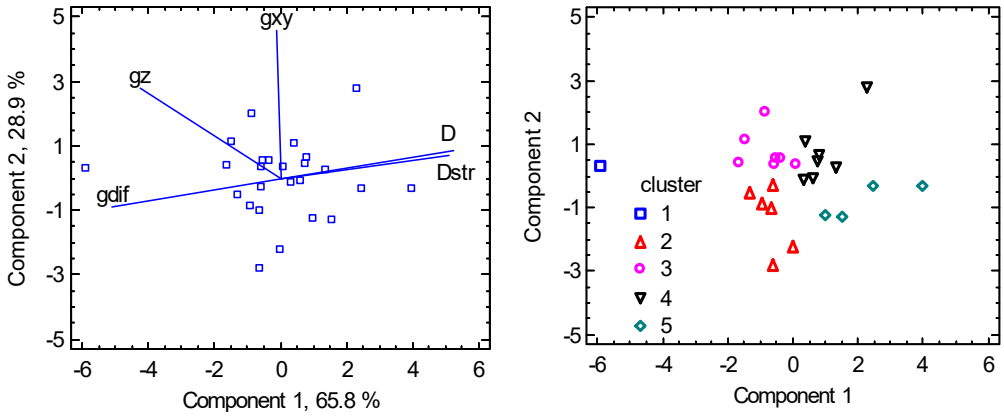


Figure 6. PCA biplot for hexacoordinate Ni(II) complexes. The points are the individual objects.

6.2. Hexacoordinate Co(II) Complexes

The above procedure outlined for Ni(II) complexes was also applied to a set of hexacoordinate Co(II) complexes. As already mentioned, only the segment of the compressed tetragonal bipyramids matches the spin-Hamiltonian formalism, and the *D*-values are expected to be very high [64].

A collection of 16 datapoints is displayed in Figure 7 (left), from which it is evident that a linear correlation does not apply in this case. This is understood from the transformed 3D graph $D = f(F_4(xy), F_4(z))$ into a 2D diagram $D = f(D_{str})$ (Figure 7, right). For the complexes with a heterogeneous coordination sphere, the mean distances $\overline{R}(\mathrm{Co-N}) = 2.185$, $\overline{R}(\mathrm{Co-O}) = 2.085$, and $\overline{R}(\mathrm{Co-Cl}) = 2.475$ Å were used to calculate the experimental D_{str} values. The data worksheet is listed in the SI and processed using multivariate statistical methods [65,66]. The Cluster Analysis based on three variables (labelled as Dstr, D2 = 2*D* and gxy) shows that the distance separates the objects into two principal clusters (Figure 8). Their separation is also well-seen from the Principal Component Analysis (Figure S2). The assumption on which the correlation 2*D* vs. D_{str} is based is thus statistically confirmed. It is clear that the discovered clustering classifies objects based on close D_{str} values, with cluster 1 including complexes with significantly more negative D_{str}. However, for the purposes of Correlation Analysis, we excluded outliers A and M from individual clusters. We assume that these objects may indicate new clusters in the segment $D_{str} < 0$. If we accept this assumption, then the non-linear correlation 2*D* vs. D_{str} has a satisfactory predictive character.

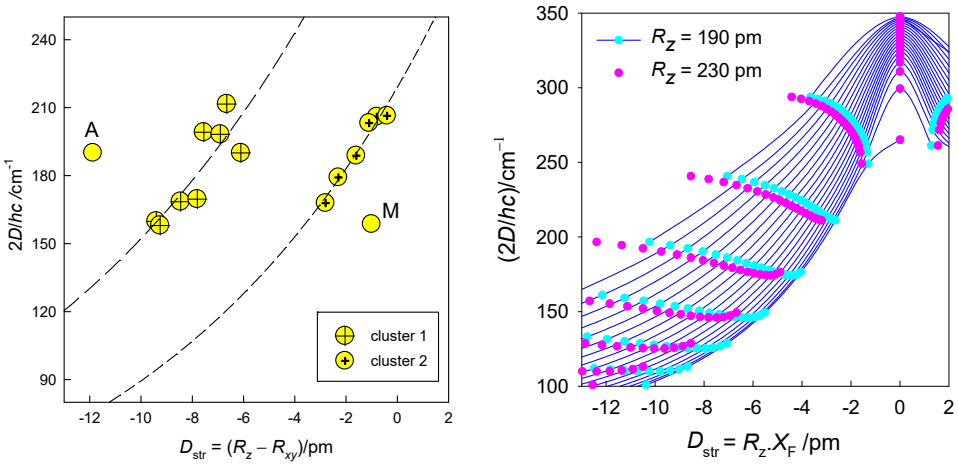


Figure 7. Magnetostructural D-correlation for hexacoordinate Co(II) complexes. Lines—fitted with an exponential $2D = b \cdot \exp(c \cdot D_{str})$ (clu 1: $b = 331.81$, $c = 0.08$, $R^2 = 0.71$, $F = 14.57$, $P = 0.009$; clu 2: $b = 218.92$, $c = 0.09$, $R^2 = 0.95$, $F = 82.63$, $P = 0.0008$). A and M were omitted from the correlation (**left**). Calculated

magnetic D-values for different equatorial–axial crystal field strengths vs. the transformed structural ordinate D_{str} for hexacoordinate Co(II) complexes. Solid lines interpolate the points for the common axial metal–ligand distance R_z = 190 pm. Pink points bracket the second limiting case, R_z = 230 pm (**right**).

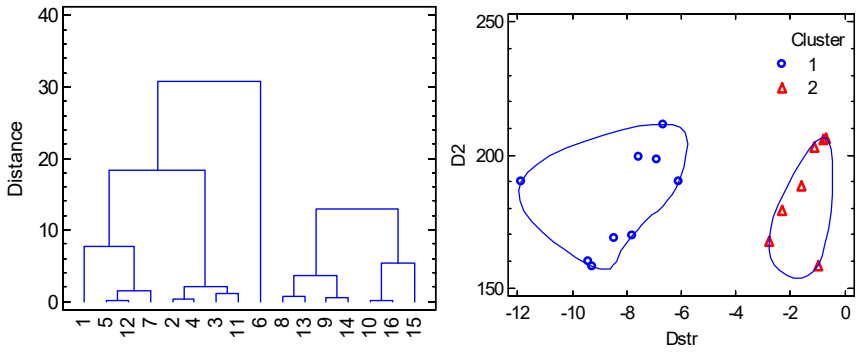


Figure 8. Cluster Analysis for hexacoordinate Co(II) complexes. Individual cluster areas are circled.

Co(II) complexes were also studied using ab initio methods (CASSCF + NEVPT2) to address the electronic origin of the ZFS and support the experimental results. This is a highly sophisticated quantum chemistry method based on the definition of multi-configurational self-consistent field (MCSCF) wave functions, which are used as reference states for multi-reference perturbation theories (MRPT), similar to n-electron valence state perturbation theory (NEVPT2) [57]. The combination of MCSCF and MRPT adequately describes multi-reference systems, such as, e.g., transition metal complexes, as it involves much of the electron correlation. In general, this approach represents a significant advance in the understanding of magnetostructural correlations, since many simpler methods based on electrostatic theories inappropriately solve the details of electronic structure-magnetism relations. It is therefore obvious that the combination of highly reliable experimental and computational techniques is currently a standard tool that, e.g., reveals how subtle structural modifications significantly affect the magnetic behaviour of molecules.

6.3. Tetracoordinate Co(II) Complexes

A collection of the spin-Hamiltonian parameters, in this case, is based upon High-Frequency/High-Field Electron Spin Resonance (syn. EPR, EMR) with 10 datapoints and completed using five results from a simultaneous fitting of the susceptibility/magnetization data for [CoA_2B_2]-type complexes [67,68]. The basic problem arises from the fact that in addition to radial variations (bond lengths Co-A, Co-B), the angular distortion (bond angles A-Co-A, B-Co-B) is substantial. Moreover, twisting angles A-Co-B come into play (in total, seven coordinates are independent).

The importance of the angular distortion was proven with modelling using the GCFT, as shown in Figure 9. The energy gap between the lowest crystal field multiplets refers to $\Delta = 2(D^2 + 3E^2)^{1/2} \doteq 2D$. On the right, the transformed ordinate was used for the 2D plot, giving rise to a general route to be followed by the magnetostructural D-correlation in tetracoordinate Co(II) complexes. It proceeds according to an increasing exponential. The correlation D vs. A_- is shown in Figure 10, and it can be concluded that the experimental data matches the general course predicted using GCFT modelling. A fit to exponential curves $D = a + b \cdot \exp(c \cdot A_-)$ is also shown with dashed lines.

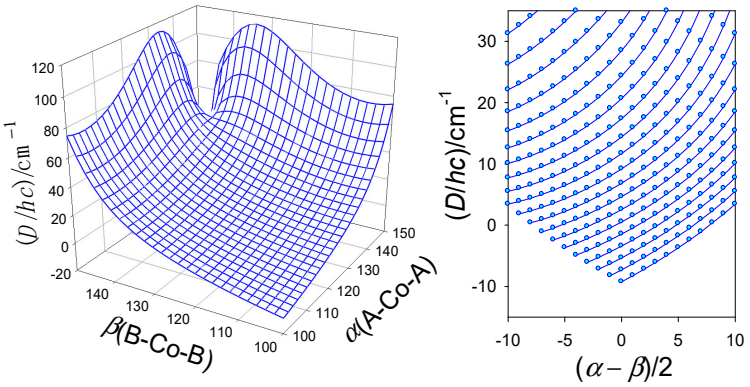


Figure 9. Calculated magnetic *D*-values (exact multiplet splitting with GCFT) for different distortion angles α(A-Co-A) and β(B-Co-B) (in deg) with fixed crystal field strengths $F_4(R)$ = 5000 cm^{-1}. (**Right**)—transformed 2D graph for an increasing angle α (from bottom to top).

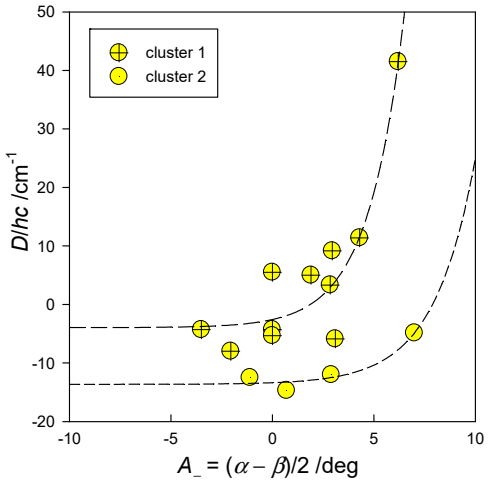


Figure 10. Magnetostructural D-correlation for tetracoordinate Co(II) complexes, $D = a + b \cdot \exp(c \cdot A_)$ (clu 1: $a = -3.95$, $b = 1.38$, $c = 0.56$, $R^2 = 0.87$, $F = 27.12$, $P = 0.0003$; clu 2: $a = -13.64$, $b = 0.27$, $c = 0.49$, $R^2 = 0.93$, $F = 7.75$, $P = 0.24$).

For the multivariate methods, seven variables were considered: *R*(Co-A), *R*(Co-B), α(A-Co-A), β(B-Co-B), g_z, g_{xy}, *D* abbreviated as RA, RB, alpha, beta, gz, gxy, and D. Also, three transformed variables were added: Aplus = (alpha + beta)/2, Aminus = (alpha − beta)/2, gdif = gz − gxy. It must be mentioned that the data involve very different chromophores as follows: {CoN_4}, {CoN_2N_2}, {$CoCl_4$}, {$CoBr_4$}, {$CoCl_2P_2$}, {$CoBr_2P_2$}, and the most numerous {$CoCl_2N_2$} one. (Two datapoints with {CoN_2O_2} and {CoO_2S_2} chromophores were deleted from consideration due to evident dissimilarity). The Cluster Analysis points to two principal clusters (Figure 11) containing 11 and 4 members, respectively. Eventually, the compound with large D/hc = 41 cm^{-1} could be classified as a new cluster. The PCA method (Figure 12) shows a rather weak correlation between the *D*-values and the individual geometric parameters; the best correlation is *D* vs. *A*_. The PCA also confirms an anticorrelation of *D* and gdif, as expected with the spin-Hamiltonian formalism. On the other hand, the PCA evidently separates the individual clusters. The non-linear correlation *D* vs. *A*_ in Figure 10 is predictive for cluster 1 but not for cluster 2. The expansion of the data in the segment of *A*_ > 0 will therefore be necessary.

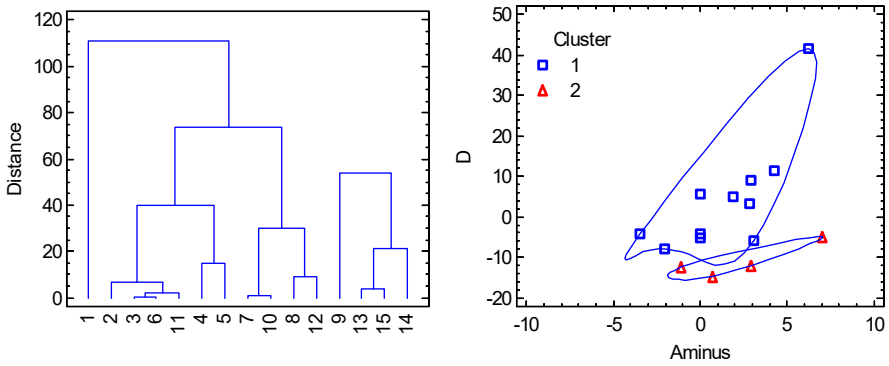


Figure 11. Cluster Analysis for tetracoordinate Co(II) complexes. Individual cluster areas are circled.

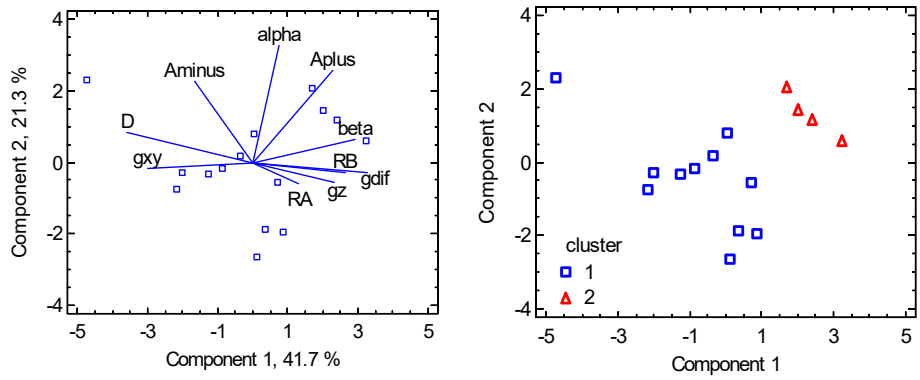


Figure 12. PCA biplot for tetracoordinate Co(II) complexes. The points are the individual objects.

6.4. Pentacoordinate Co(II) Complexes

For pentacoordinate complexes of the [$CoXA_2B_2$] type, a basic obstacle arises from the fact that too many (12) geometrical parameters come into play, and the coordination polyhedron is often far from the ideal tetragonal pyramid and/or trigonal bipyramid. Also, the description of the intermediate geometries with the angular distortion (trigonality) τ-parameter represents a strong idealization. Moreover, there are only a few reliable magnetic datapoints based on both the susceptibility and magnetization measurements (HF/HF EPR cannot be used since *D*-values are too large).

The angular dependence of the *D*-parameter with respect to two geometrical parameters is shown in Figure 13. The polar angles θ(A) and θ(B) were used to map the Berry-kind of transformation between the trigonal bipyramid and tetragonal pyramid using GCFT. It is worth noting the fact that the majority of the complexes under study possess trigonality parameter $\tau > 1$ due to a rigid tridentate ligand with the {XA_2} donor set.

Eleven datapoints were collected (see the Supplementary Material) [69,70] and the variables *R*(Co-X), *R*(Co-A), *R*(Co-B), α(A-Co-A), β(B-Co-B), θ(X-Co-A), θ(X-Co-B), *D*, and g_{xy} are abbreviated for statistical analysis as RX, RA, RB, alpha, beta, thetaA, thetaB, D, and gxy. Moreover, three transformed variables were considered: $\gamma = 360 - 2\theta$(A), $\tau = (\alpha - \beta)/60$ or $\tau = (\gamma - \beta)/60$ when $\gamma > 180$ deg, and $\delta = (\alpha - \beta)/2$ abbreviated as gamma, tau, and dis. The cluster analysis distinguishes two main clusters with eight and three datapoints, respectively (Figure 14). For the first cluster, $\gamma > 180$ deg and $\tau > 1$ holds true; for the second cluster: $\gamma < 180$ deg, $\tau < 1$. The PCA revealed a significant correlation between parameter *D* and parameters *R*(Co-X), *R*(Co-B), and g_x; however, this does not provide more fundamental information in this case. Rather, a weak positive correlation with the γ parameter and anticorrelation with α appear to be more significant. Moreover, the PCA again visibly separates two clusters (Figure 15).

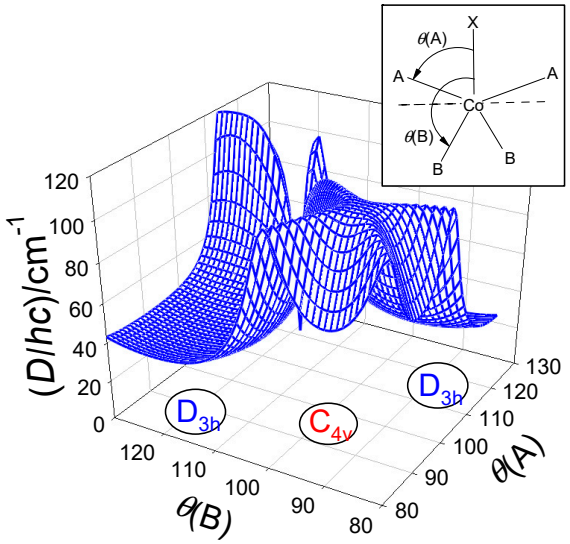


Figure 13. Calculated magnetic D-values (exact multiplet splitting with GCFT) for polar angles θ(A) and θ(B) (in deg) with fixed crystal field strengths $F_4(R)$ = 6000 cm^{-1}.

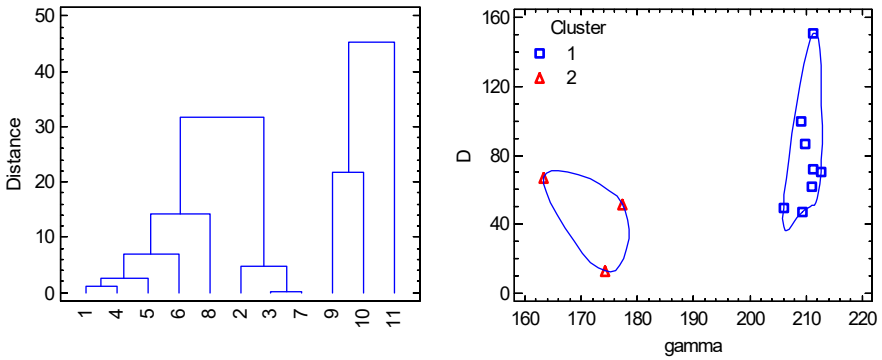


Figure 14. Cluster Analysis for pentacoordinate Co(II) complexes. Individual cluster areas are circled.

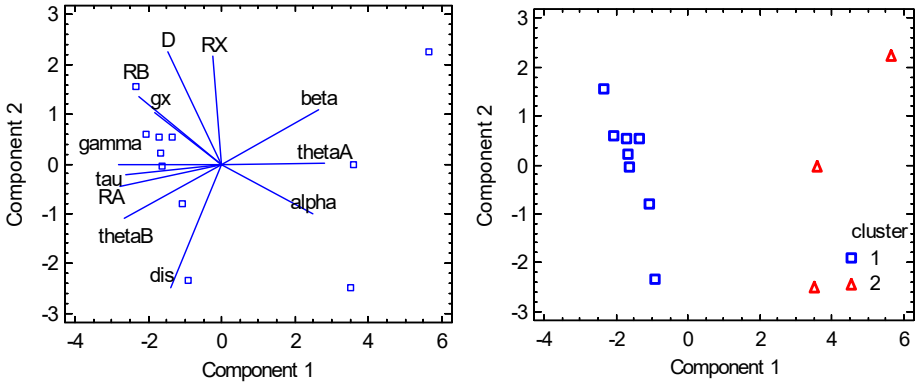


Figure 15. PCA biplot for pentacoordinate Co(II) complexes. The points are the individual objects.

A trial set of functions to fit the observed D vs. structural parameter relationships is shown in Figure 16. Notice that the actual geometry is far from an ideal polyhedron, where a crude averaging of bond angles was applied. Moreover, some of the [Co(L^{Cn})Cl$_2$] systems form a supramolecular dimer with exchange interaction $J > 0$. In such a case, the local D-tensors are not necessarily collinear, and this circumstance affects the fitted D-values. The correlation coefficient between D and g_x (r = 0.83) proves that the spin-Hamiltonian formula $D = \lambda(g_z - g_x)/2$ is fulfilled for pentacoordinate complexes. This conclusion matches the forecast that only $D > 0$ applies for pentacoordinate Co(II) complexes [71]. In this light, the

reported values of $D/hc = -40$ cm^{-1} in $\{CoN_2N_3\}$-type complexes seem be problematic: the authors fail in fitting the magnetization data and, moreover, they used closed formula for the addition of three Cartesian components, and neither their average nor a correct powder average was applied [72].

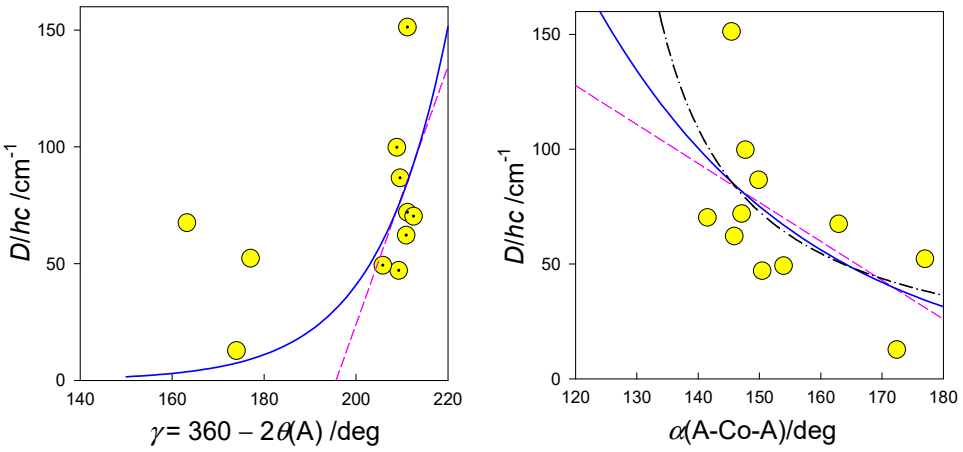


Figure 16. Magnetostructural D-correlation for pentacoordinate Co(II) complexes. Trial correlation curves: dashed-linear, solid-exponential $y = a \cdot \exp(bx)$, dot-dashed $y = y_0 + a/(x - x_0)$.

7. Selected Single-Molecule Magnets

The list of known single-molecule magnets based upon one metal centre (single-ion magnets, SIM) is rapidly increasing. They cover, for instance, Mn(III), Mn(II), Fe(III), Fe(II), Fe(I), Co(II), Ni(III), and Ni(II) complexes [73–89]. Representative examples for Co(II) are presented in Table 1. It is worth noting that there is an inverse relationship between the extrapolated relaxation time $\ln\tau_0$ and barrier to spin reversal U, as shown in Figure 17.

Table 1. List of single-molecule (single-ion) magnets containing Co(II).

C.n.	Chromophore	Geometry [a]	(D/hc)/cm^{-1}	(E/hc)/cm^{-1}	B_{DC}/T	(U/k_B)/K	τ_0/s	Ref.
3	$\{CoN_3\}$		−57	12.7	0.08	16	3.5×10^{-7}	[82]
	$\{CoN_2O\}$		−72	13.5	0.06	18	9.3×10^{-8}	[82]
	$\{CoN_2P\}$		−82		0.075	19	3.0×10^{-7}	[82]
4	$\{CoS_4\}$		−74		0.10	30	1.0×10^{-7}	[83]
	$\{CoN_3Cl\}$		+12.7	1.2	0.15	35	2×10^{-10}	[84]
	$\{CoP_2Cl_2\}$		−16.2	0.9	0.10	37	1.2×10^{-10}	[85]
	$\{CoP_2Cl_2\}$		−14.4	1.7	0.10	35	2.1×10^{-10}	[85]
	$\{CoP_2Cl_2\}$		−15.4	1.3	0.10	30	6.0×10^{-9}	[85]
	$\{CoP_2Br_2\}$		−12.5		0.10	37	9.4×10^{-11}	[86]
					0.20	40	6.0×10^{-11}	[86]
5	$\{CoN_3N_2\}$	4py	−40.5	$J > 0$	0.20	16	3.6×10^{-6}	[86]
	$\{CoN_3N_2\}$	4py	−40.6		0.20	24	5.1×10^{-7}	[72]
	$\{CoN_3N_2\}$	3bpy	(+49.0), calc		0.06	17	5.85×10^{-6}	[90]
					0.56	3	0.110	[90]
	$\{CoN_3Cl_2\}$	4py	(+99.5), calc		0.06	28	1.1×10^{-6}	[90]
					0.56	4	0.074	[90]
	$\{CoN_3Cl_2\}_2$	4py	151	11.6, $J > 0$	0.20	9	3.1×10^{-7}	[69]
					0.20	1	0.27	[69]
6	$\{CoN_4N_2\}$		+48	13.0	0.30	83	8.7×10^{-10}	[64]
	$\{CoN_4N_2\}$		+98	8.4	0.10	23	3.0×10^{-7}	[72]
	$\{CoO_3N_3\}$		+41.7	1.6	0.10	23	8.9×10^{-7}	[88]
	$\{CoO_6\}$		−115	2.8	0	106	1.7×10^{-7}	[89]
					0.15	124	6.3×10^{-8}	[89]

[a] C.n.—coordination number; 4py—tetragonal pyramid, 3bpy—trigonal bipyramid; calc—estimate from the calculated energy gap between the lowest Kramer doublets as $\Delta = 2(D^2 + 3E^2)^{1/2} \sim 2D$.

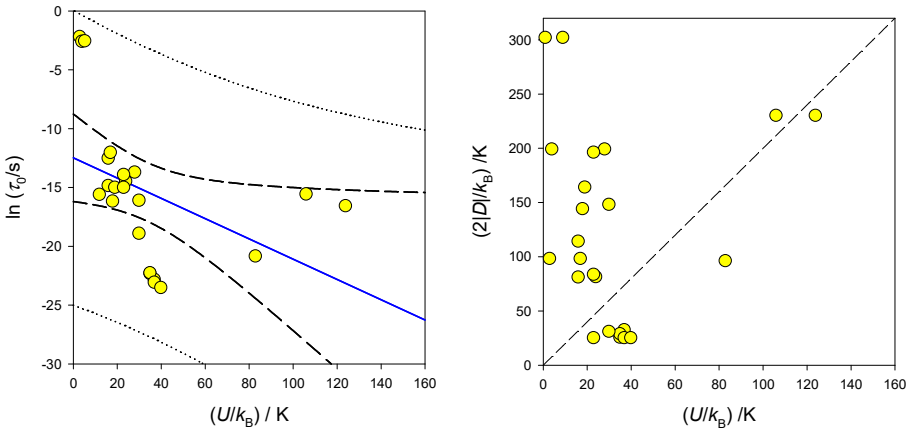


Figure 17. A relationship between the barrier to spin reversal and the extrapolated relaxation time in SIM containing Co(II). (**Right**)-interrelation between D and U (dashed-expected $U = 2|D|$).

The existence of the barrier to spin reversal is traditionally expected only for $D < 0$ (easy-axis of magnetization). However, SMM (SIM) behaviour was also registered in the case of $D > 0$; a presence of sufficient rhombic anisotropy ($E > 0$) rationalizes this observation. In this case, the easy-plane allowing unhindered relaxation no longer exists; a small barrier to spin reversal is determined by the E parameter.

The above outlined magnetostructural correlations allow us to predict whether the system under study is a potential candidate for single-molecule magnetism. For instance, the observed value of $D/hc = -12.5$ cm^{-1} in a $[Co(PPh_3)_2Br_2]$ complex from the DC magnetization studies motivated the AC susceptibility measurements and, indeed, the SMM behaviour was confirmed [86].

The expected relationship for the half-integral spin $S = 3/2$ is $U = 2|D_S|$ (in the zero field), and this is evidently not obeyed (Figure 17). The way of extracting the SMM parameters is also questionable: usually, they arise from the Arrhenius-like linear relationship $\ln \tau = \ln \tau_0 + (U/k_B)T^{-1}$ applied to higher-temperature points. However, a more complex equation that involves the Raman, direct, and quantum tunnelling processes is available

$$\tau^{-1} = \tau_0^{-1} \exp(-U/k_B T) + CT^n + AB^2T + D(B) \quad (38)$$

This can be enriched by the phonon bottleneck effect FT^2 and the reciprocating thermal behaviour term GT^{-1}.

Some samples exhibit multiple relaxation processes that vary with the applied magnetic field, so it is problematic to relate single D-values with different U-values. The presence of various relaxation processes is visible only if a search for them is applied, e.g., for low ($\nu < 1$ Hz) or high ($\nu > 1500$ Hz) frequencies of the AC field. Co(II) complexes represent a rich class of single-ion magnets. These exhibit large magnetic anisotropy that necessarily is positive for a compressed tetragonal bipyramid. The Orbach relaxation mechanism, however, requires $D < 0$. For (pseudo)octahedral systems, we found that the ZFS parameter D, and thus magnetic anisotropy, strongly decreases with tetragonal distortion. For near-octahedral structures, the D-parameter achieves large positive values (up to 350 cm^{-1} for ideal O_h—Jahn–Teller systems). Hexacoordinate Co(II) complexes with markedly negative D-values were also reported [91,92]. An example is also $(HNEt_3)^+(Co^{II}Co^{III}{}_3L_6)^-$, $D/hc = -115$ cm^{-1}. However, the symmetry of this structure is D_3 [89].

8. Summary

Magnetostructural D-correlations, i.e., dependence of the axial zero-field splitting parameter D vs. the structural anisotropy parameter D_{str}, originate in the electronic structure of the central atom. They are tuned by the ligand diversity and structural variability in the individual metal complexes. Intuitive linear relationships (as in hexacoordinate Ni(II)

systems) are not always supported with deep theoretical analysis, which can rationalize various types of non-linear dependencies. This is the case of the hexa-, penta-, and tetra-coordinate Co(II) complexes. Magnetostructural D-correlations represent an effective tool for the design of magnetically anisotropic molecules. Only from the knowledge of the structural characteristics of the complexes can the magnitude and sign of the axial zero-field splitting parameter *D* be predicted, which enables the creation of relevant prediction models using contemporary machine learning methods [93].

Supplementary Materials: The following supporting information can be downloaded at: https://www.mdpi.com/article/10.3390/inorganics11120452/s1, Figure S1: FA biplot after varimax rotation for hexacoordinate Ni(II) complexes; Figure S2: PCA biplot for hexacoordinate Co(II) complexes; Table S1: Review of the matrix elements among atomic-term kets; Table S2: Energy level diagrams for selected d^n systems; Table S3: Hexacoordinate Ni(II) complexes—structural and magnetic parameters and statistics; Table S4: Hexcoordinate Co(II) complexes—structural and magnetic parameters and statistics; Table S5: Tetracoordinate Co(II) complexes—structural and magnetic parameters and statistics; Table S6: Pentacoordinate Co(II) complexes—structural and magnetic parameters and statistics; data selections for multivariate methods [94].

Author Contributions: Conceptualization, J.T. and R.B.; methodology, J.T. and R.B.; validation, J.T., R.B. and C.R.; formal analysis, J.T., R.B. and C.R.; investigation, J.T., R.B. and C.R.; data curation, J.T., R.B., and C.R.; writing—original draft preparation, J.T., R.B. and C.R.; writing—review and editing, J.T., R.B. and C.R.; visualization, J.T., R.B. and C.R. All authors have read and agreed to the published version of the manuscript.

Funding: This research received no external funding.

Data Availability Statement: All relevant experimental data are provided in the Supporting Information. Protocols of the CGTF and ab initio calculations are available from authors upon reasonable request.

Acknowledgments: Slovak Research and Development Agency (APVV 19-0087 and VEGA 1/0086/21) are acknowledged for their financial support.

Conflicts of Interest: The authors declare no conflict of interest.

References

1. Lis, T. Preparation, structure, and magnetic properties of a dodecanuclear mixed-valence manganese carboxylate. *Acta Crystallogr.* **1980**, *B36*, 2042–2046. [CrossRef]
2. Caneschi, A.; Gatteschi, D.; Sessoli, R.; Barra, A.L.; Brunel, L.C.; Guillot, L.C. Alternating current susceptibility, high field magnetization, and millimeter band EPR evidence for a ground S = 10 state in $[Mn_{12}O_{12}(Ch_3COO)_{16}(H_2O)_4]\cdot_2CH_3COOH.{}_4H_2O$. *J. Am. Chem. Soc.* **1991**, *133*, 5873–5874. [CrossRef]
3. Aubin, S.M.J.; Wemple, M.W.; Adams, D.M.; Tsai, H.L.; Christou, G.; Hendrickson, D.N. Distorted MnIVMnIII3 Cubane Complexes as Single-Molecule Magnets. *J. Am. Chem. Soc.* **1996**, *118*, 7746–7754. [CrossRef]
4. Gatteschi, D.; Sessoli, R.; Villain, J. *Molecular Nanomagnets*; Oxford University Press: Oxford, UK, 2006.
5. Affronte, M. Molecular Nanomagnets for Information Technologies. *J. Mater. Chem.* **2009**, *19*, 1731–1737. [CrossRef]
6. Lumetti, S.; Candini, A.; Godfrin, C.; Balestro, F.; Wernsdorfer, W.; Klyatskaya, S.; Ruben, M.; Affronte, M. Single-Molecule Devices with Graphene Electrodes. *Dalton Trans.* **2016**, *45*, 16570–16574. [CrossRef]
7. Milios, C.J.; Winpenny, R.E.P. Cluster-Based Single-Molecule Magnets. *Struct. Bond.* **2015**, *164*, 1–109.
8. Coronado, E. Molecular Magnetism: From Chemical Design to Spin Control in Molecules, Materials and Devices. *Nat. Rev. Mater.* **2020**, *5*, 87–104. [CrossRef]
9. Shao, D.; Wang, X.Y. Development of Single-Molecule Magnets†. *Chin. J. Chem.* **2020**, *38*, 1005–1018. [CrossRef]
10. Layfield, R.A. Organometallic Single-Molecule Magnets. *Organometallics* **2014**, *33*, 1084–1099. [CrossRef]
11. Wernsdorfer, W.; Sessoli, R. Quantum Phase Interference and Parity Effects in Magnetic Molecular Clusters. *Science* **1999**, *284*, 133–135. [CrossRef]
12. Coulon, C.; Miyasaka, H.; Clérac, R. Single-Chain Magnets: Theoretical Approach and Experimental Systems. Struct. *Bonding* **2006**, *122*, 163–206. [CrossRef]
13. Mydosh, J.A. *Spin Glasses: An Experimental Introduction*; Taylor and Francis: London, UK, 1995.
14. Winpenny, R. (Ed.) *Single-Molecule Magnets and Related Phenomena, Structure and Bonding*; Springer: Berlin/Heidelberg, Germany, 2006; p. 122.
15. Fu, Z.; Qin, L.; Sun, K.; Hao, L.; Zheng, Y.-Z.; Lohstroh, W.; Günther, G.; Russina, M.; Liu, Y.; Xiao, Y.; et al. Low-temperature spin dynamics of ferromagnetic molecular ring {Cr8Y8}. *NPJ Quantum Mater.* **2020**, *5*, 32. [CrossRef]

16. Garlatti, E.; Albring, M.A.; Baker, M.L.; Docherty, R.J.; Mutka, H.; Guidi, T.; Garcia, S.V.; Whitehead, G.F.; Pritchard, R.G.; Timco, G.A.; et al. A detailed study of the magnetism of chiral {Cr_7M} rings: An investigation into parametrization and transferability of parameters. *J. Am. Chem. Soc.* **2014**, *136*, 9763–9772. [CrossRef]
17. Low, D.M.; Rajaraman, G.; Helliwell, M.; Timco, G.; van Slageren, J.; Sessoli, R.; Ochsenbein, S.T.; Bircher, R.; Dobe, C.; Waldmann, O.; et al. A family of ferro- and antiferromagnetically coupled decametallic chromium(III) wheels. *Chemistry* **2006**, *12*, 1385–1396. [CrossRef]
18. Miyasaka, H.; Madanbashi, T.; Saitoh, A.; Motokawa, N.; Ishikawa, R.; Yamashita, M.; Bahr, S.; Wernsdorfer, W.; Clérac, R. Cyano-Bridged MnIII-MIII Single-Chain Magnets with MIII=CoIII, FeIII, MnIII, and CrIII. *Chem. Eur. J.* **2012**, *18*, 3942–3954. [CrossRef]
19. Boskovic, C.; Brechin, E.K.; Streib, W.E.; Folting, K.; Bollinger, J.C.; Hendrickson, D.N.; Christou, G. Single-molecule magnets: A new family of Mn12 clusters of formula [$Mn_{12}O_8X_4$ $(O_2CPh)_8L_6$]. *J. Am. Chem. Soc.* **2002**, *124*, 3725–3736. [CrossRef]
20. Moushi, E.E.; Stamatatos, T.C.; Wernsdorfer, W.; Nastopoulos, V.; Christou, G.; Tasiopoulos, A.J. A Mn17 Octahedron with a Giant Ground-State Spin: Occurrence in Discrete Form and as Multidimensional Coordination Polymers. *Inorg. Chem.* **2009**, *48*, 5049–5051. [CrossRef]
21. Ghulam Abbas, G.; Lan, Y.; Mereacre, V.; Wernsdorfer, W.; Clerac, R.; Buth, G.; Sougrati, M.T.; Grandjean, F.; Long, G.J.; Anson, C.E.; et al. Magnetic and 57Fe Mössbauer Study of the Single Molecule Magnet Behavior of a Dy3Fe7 Coordination Cluster. *Inorg. Chem.* **2009**, *48*, 9345–9355. [CrossRef]
22. Morello, A.; Mettes, F.L.; Luis, F.; Fernández, F.J.; Krzystek, J.; Aromí, G.; Christou, G.; de Jongh, L.J. Long-range dipolar ferromagnetic ordering of high-spin molecular clusters. *Phys. Rev. Lett.* **2003**, *90*, 017206. [CrossRef]
23. Burzuri, E.; Luis, F.; Barbara, B.; Ballou, R.; Ressouche, E.; Montero, O.; Campo, J.; Maegawa, S. Magnetic dipolar ordering and quantum phase transition in an Fe8 molecular magnet. *Phys. Rev. Lett.* **2011**, *107*, 097203. [CrossRef]
24. Goodwin, J.C.; Sessoli, R.; Gatteschi, D.; Wernsdorfer, W.; Powell, A.K.; Heath, S.L. Towards nanostructured arrays of single molecule magnets: New Fe19 oxyhydroxide clusters displaying high ground state spins and hysteresis. *J. Chem. Soc. Dalton Trans.* **2020**, *12*, 1835–1840. [CrossRef]
25. Affronte, M.; Lasjaunias, J.C.; Wernsdorfer, W.; Sessoli, R.; Gatteschi, D.; Heath, S.L.; Fort, A.; Rettori, A. Magnetic ordering in a high-spin Fe19 molecular nanomagnet. *Phys. Rev. B* **2002**, *66*, 064408. [CrossRef]
26. Affronte, M.; Sessoli, R.; Gatteschi, D.; Wernsdorfer, W.; Lasjaunias, J.C.; Heath, S.L.; Powell, A.K.; Fort, A.; Rettori, A. Effects of intercluster coupling in high spin molecular magnets. *J. Phys. Chem. Sol.* **2004**, *65*, 745–748. [CrossRef]
27. Bogani, L.; Wernsdorfer, W. Molecular spintronics using single-molecule magnets. *Nat. Mater.* **2008**, *7*, 179–186. [CrossRef] [PubMed]
28. Miyasaka, H.; Clerac, R. Synthetic Strategy for Rational Design of Single-Chain Magnets. *Bull. Chem. Soc. Jpn.* **2005**, *78*, 1725–1748. [CrossRef]
29. Miyasaka, H.H.; Takahashi, M.T.; Sugiura, K.; Clérac, R.; Nojiri, H. Cyano-Bridged MnIII3MIII (MIII = Fe, Cr) Complexes: Synthesis, Structure, and Magnetic Properties. *Inorg. Chem.* **2005**, *44*, 5969–5971. [CrossRef]
30. Boča, R.; Rajnák, C. Unexpected behavior of single ion magnets. *Coord. Chem. Rev.* **2021**, *430*, 213657. [CrossRef]
31. Craig, G.A.; Murrie, M. 3d single-ion magnets. *Chem. Soc. Rev.* **2015**, *44*, 2135–2147. [CrossRef] [PubMed]
32. Meng, Y.-S.; Jiang, S.-D.; Wang, B.-W.; Gao, S. Understanding the Magnetic Anisotropy Toward Single-ion Magnets. *Acc. Chem. Res.* **2016**, *49*, 2381–2389. [CrossRef]
33. Atzori, M.; Tesi, L.; Morra, E.; Chiesa, M.; Sorace, L.; Sessoli, R. Room-Temperature Quantum Coherence and Rabi Oscillations in Vanadyl Phthalocyanine: Toward Multifunctional Molecular Spin Qubits. *J. Am. Chem. Soc.* **2016**, *138*, 2154–2157. [CrossRef]
34. Ding, M.; Cutsail, G.E.I.; Aravena, D.; Amoza, M.; Rouzières, M.; Dechambenoit, P.; Losovyj, Y.; Pink, M.; Ruiz, E.; Clérac, R. A low spin manganese(iv) nitride single molecule magnet. *Chem. Sci.* **2016**, *7*, 6132–6140. [CrossRef] [PubMed]
35. Bhowmick, I.; Shaffer, D.W.; Yang, J.Y.; Shores, M.P. Single molecule magnet behaviour in a square planar S = 1/2 Co(ii) complex and spin-state assignment of multiple relaxation modes. *Chem. Commun.* **2020**, *56*, 6711–6714. [CrossRef] [PubMed]
36. Chen, L.; Song, J.; Zhao, W.; Yi, G.; Zhou, Z.; Yuan, A.; Song, Y.; Wang, Z.; Ouyang, Z.W. A mononuclear five-coordinate Co(ii) single molecule magnet with a spin crossover between the S = 1/2 and 3/2 states. *Dalton Trans.* **2018**, *47*, 16596–16602. [CrossRef] [PubMed]
37. Boča, R. *A Handbook of Magnetochemical Formulae*; Elsevier: Amsterdam, The Netherlands, 2012.
38. Griffith, J.S. *The Theory of Transition Metal Ions*; Cambridge University Press: Cambridge, CA, USA, 1964.
39. Figgis, B.N. *Introduction to Ligand Fields*; Wiley: New York, NY, USA, 1966.
40. König, E.; Kremer, S. *Magnetism Diagrams for Transition Metal Ions*; Plenum Press: New York, NY, USA, 1979.
41. König, E.; Kremer, S. Irreducible tensor operator methods in intermediate-field coupling. *Int. J. Quant. Chem.* **1974**, *8*, 347–362. [CrossRef]
42. König, E.; Kremer, S. Irreducible Tensor Operator Methods in Strong-field Coupling. *Int. J. Quant. Chem.* **1977**, *12*, 1017–1031. [CrossRef]
43. Boča, R. *Program MIF&FIT*; University of SS Cyril and Methodius: Trnava, Slovakia, 2022.
44. Crawford, V.H.; Richardson, H.W.; Wasson, J.R.; Hodgson, D.J.; Hatfield, W.E. Relation between the singlet-triplet splitting and the copper-oxygen-copper bridge angle in hydroxo-bridged copper dimers. *Inorg. Chem.* **1976**, *15*, 2107–2110. [CrossRef]

45. Hatfield, W.E.; Willett, R.D.; Gatteschi, D.; Kahn, O. *Magneto-Structural Correlations in Exchange Coupled Systems*; NATO ASI Series Reidel: Dordrecht, The Netherlands, 1985.
46. Thompson, L.K.; Mandal, S.K.; Tandon, S.S.; Bridson, J.N.; Park, M.K. Magnetostructural Correlations in Bis(μ2-phenoxide)-bridged Macrocyclic Dinuclear Copper(ii) Complexes. Influence of Electron-withdrawing Substituents on Exchange Coupling. *Inorg. Chem* **1996**, *35*, 3117–3125. [CrossRef]
47. Glerup, J.; Hodgson, D.J.; Pedersen, E. A Novel Correlation Between Magnetism and Structural Parameters in Superexchange Coupled Chromium(iii) Dimers. *Acta. Chem. Scand.* **1983**, *37a*, 161–164. [CrossRef]
48. Law, N.A.; Kampf, J.W.; Pecoraro, V.L. A magneto-structural correlation between the Heisenberg constant, J, and the Mn-O-Mn angle in $[MnIV(\mu\text{-}O)]_2$ dimers. *Inorg. Chim. Acta.* **2000**, *297*, 252–264. [CrossRef]
49. Gorun, S.M.; Lippard, S.J. Magnetostructural Correlations in Magnetically Coupled (.mu.-oxo)diiron(iii) Complexes. *Inorg. Chem.* **1991**, *30*, 1625–1630. [CrossRef]
50. Werner, R.; Ostrovsky, S.; Griesar, K.; Haase, W. Magnetostructural Correlations in Exchange Coupled Phenoxo-, Alkoxo-, and Hydroxo-bridged Dinuclear Iron(iii) Compounds. *Inorg. Chim. Acta* **2001**, *326*, 78–88. [CrossRef]
51. Mitchell, K.J.; Abboud, K.A.; Christou, G. Magnetostructural Correlation for High-Nuclearity Iron(III)/Oxo Complexes and Application to Fe5, Fe6, and Fe8 Clusters. *Inorg. Chem.* **2016**, *55*, 6597–6608. [CrossRef] [PubMed]
52. Makohusová, M.; Mrázová, V.; Haase, W.; Boča, R. Magnetostructural J-correlations in complexes with tetrahedro-{Cu4} core. *Polyhedron* **2014**, *81*, 572–582. [CrossRef]
53. Neese, F.; Solomon, R.I. Calculation of Zero-Field Splittings, g-Values, and the Relativistic Nephelauxetic Effect in Transition Metal Complexes. Application to High-Spin Ferric Complexes. *Inorg. Chem.* **1998**, *37*, 6568–6582. [CrossRef] [PubMed]
54. Maganas, D.; Krzystek, J.; Ferentinos, E.; Whyte, A.M.; Robertson, N.; Psycharis, V.; Terzis, A.; Neese, F.; Kyritsis, P. Investigating Magnetostructural Correlations in the Pseudooctahedral Trans-[niii{(opph2)(epph2)n}2(sol)2] Complexes (E = S, Se; Sol = DMF, THF) by Magnetometry, HFEPR, and Ab Initio Quantum Chemistry. *Inorg. Chem.* **2012**, *51*, 7218–7231. [CrossRef] [PubMed]
55. Duboc, C.; Ganyushin, D.; Sivalingam, K.; Collomb, M.-N.; Neese, F. Systematic Theoretical Study of the Zero-field Splitting in Coordination Complexes of Mn(iii). Density Functional Theory Versus Multireference Wave Function Approaches. *J. Phys. Chem. A* **2010**, *114*, 10750–10758. [CrossRef] [PubMed]
56. Carlin, R.L. *Magnetochemistry*; Springer: Berlin/Heidelberg, Germany, 1986.
57. Ganyushin, D.; Neese, F. First-principles calculations of zero-field splitting parameters. *J. Chem. Phys.* **2006**, *125*, 024103. [CrossRef]
58. König, E.; Schnakig, R. Zero-field splitting of 6S(d5) ions in tetragonal and rhombic symmetry: I. Complete d-electron calculation of the crystal-field dependence of D and E. *Phys. Status Solidi (b)* **1976**, *77*, 657–666. [CrossRef]
59. Neese, F. Importance of Direct Spin−spin Coupling and Spin-flip Excitations for the Zero-field Splittings of Transition Metal Complexes: A Case Study. *J. Am. Chem. Soc.* **2006**, *128*, 10213–10222. [CrossRef]
60. *SigmaPlot*; Version 10.0; Systat Software, Inc.: San Jose, CA, USA, 2013.
61. Boča, R.; Titiš, J. *Coordination Chemistry Research Progress*; Nova Science Publishers: New York, NY, USA, 2008; p. 247.
62. Titiš, J.; Boča, R. Magnetostructural D Correlation in Nickel(II) Complexes: Reinvestigation of the Zero-Field Splitting. *Inorg. Chem.* **2010**, *49*, 3971–3973. [CrossRef]
63. *Statgraphics*; Centurion XV Version 15.2.06.; StatPoint, Inc.: Herndon, VA, USA, 2007.
64. Herchel, R.; Váhovská, L.; Potočňák, I.; Trávníček, Z. Slow Magnetic Relaxation in Octahedral Cobalt(II) Field-Induced Single-Ion Magnet with Positive Axial and Large Rhombic Anisotropy. *Inorg. Chem.* **2014**, *53*, 5896–5898. [CrossRef]
65. Titiš, J.; Boča, R. Magnetostructural D Correlations in Hexacoordinated Cobalt(ii) Complexes. *Inorg. Chem.* **2011**, *50*, 11838–11845. [CrossRef]
66. Papánková, B.; Boča, R.; Dlháň, Ľ.; Nemec, I.; Titiš, J.; Svoboda, I.; Fuess, H. Magneto-structural relationships for a mononuclear Co(II) complex with large zero-field splitting. *Inorg. Chim. Acta* **2010**, *363*, 147–156. [CrossRef]
67. Idešicová, M.; Titiš, J.; Krzystek, J.; Boča, R. Zero-Field Splitting in Pseudotetrahedral Co(II) Complexes: A Magnetic, High-Frequency and -Field EPR, and Computational Study. *Inorg. Chem.* **2013**, *52*, 9409–9417. [CrossRef]
68. Titiš, J.; Miklovič, J.; Boča, R. Magnetostructural study of tetracoordinate cobalt(II) complexes. *Inorg. Chem. Commun.* **2013**, *35*, 72–75. [CrossRef]
69. Rajnák, C.; Titiš, J.; Šalitroš, I.; Boča, R.; Fuhr, O.; Ruben, M. Zero-field splitting in pentacoordinate Co(II) complexes. *Polyhedron* **2013**, *65*, 122–128. [CrossRef]
70. Rajnák, C.; Titiš, J.; Fuhr, O.; Ruben, M.; Boča, R. Single-Molecule Magnetism in a Pentacoordinate Cobalt(II) Complex Supported by an Antenna Ligand. *Inorg. Chem.* **2014**, *53*, 8200–8202. [CrossRef]
71. Makinen, M.V.; Kuo, L.C.; Yim, M.B.; Wells, G.B.; Fukuyama, J.M.; Kim, J.E. Ground Term Splitting of High-spin Cobalt(2+) Ion as a Probe of Coordination Structure. 1. Dependence of the Splitting on Coordination Geometry. *J. Am. Chem. Soc.* **1985**, *107*, 5245–5255. [CrossRef]
72. Jurca, T.; Farghal, A.; Lin, P.-H.; Korobkov, I.; Murugesu, M.; Richeson, D.S. Single-Molecule Magnet Behavior with a Single Metal Center Enhanced through Peripheral Ligand Modifications. *J. Am. Chem. Soc.* **2011**, *133*, 15814–15817. [CrossRef]
73. Ishikawa, R.; Miyamoto, R.; Nojiri, H.; Breedlove, B.K.; Yamashita, M. Slow Relaxation of the Magnetization of an MnIII Single Ion. *Inorg. Chem.* **2013**, *52*, 8300–8302. [CrossRef]

74. Grigoropoulous, A.; Pissas, M.; Rapatolis, P.; Psycharis, V.; Kyritsis, P.; Sanakis, Y. Spin-relaxation Properties of a High-spin Mononuclear Mniiio6-containing Complex. Spin-Relaxation Properties of a High-Spin Mononuclear MnIIIO6-Containing Complex. *Inorg. Chem.* **2013**, *52*, 12869–12871. [CrossRef]
75. Vallejo, J.; Pascual-Alvarez, A.; Cano, J.; Castro, I.; Julve, M.; Lloret, F.; Krzystek, J.; De Munno, G.; Armentano, D.; Wernsdorfer, W.; et al. Field-induced Hysteresis and Quantum Tunneling of the Magnetization in a Mononuclear Manganese(iii) Complex. Field-Induced Hysteresis and Quantum Tunneling of the Magnetization in a Mononuclear Manganese(III) Complex. *Angew. Chem. Int. Ed.* **2013**, *125*, 14325–14329. [CrossRef]
76. Mossin, S.; Tran, B.L.; Adhikari, D.; Pink, M.; Heinemann, F.W.; Sutter, J.; Szilagyi, R.K.; Meyer, K.; Mindiola, D.J. A Mononuclear Fe(III) Single Molecule Magnet with a 3/2↔5/2 Spin Crossover. *J. Am. Chem. Soc.* **2012**, *134*, 13651–13661. [CrossRef] [PubMed]
77. Harman, W.H.; Harris, T.D.; Freedman, D.E.; Fong, H.; Chang, A.; Rinehart, J.D.; Ozarowski, A.; Sougrati, M.T.; Grandjean, F.; Long, G.J.; et al. Slow Magnetic Relaxation in a Family of Trigonal Pyramidal Iron(ii) Pyrrolide Complexes. Slow Magnetic Relaxation in a Family of Trigonal Pyramidal Iron(II) Pyrrolide Complexes. *J. Am. Chem. Soc.* **2010**, *132*, 18115–18126. [CrossRef]
78. Freedman, D.E.; Harman, W.H.; Harris, T.D.; Long, G.J.; Chang, C.J.; Long, J.R. Slow Magnetic Relaxation in a High-spin Iron(ii) Complex. *J. Am. Chem. Soc.* **2010**, *132*, 1224–1225. [CrossRef]
79. Weismann, D.; Sun, Y.; Lan, Y.; Wolmershauser, G.; Powell, A.K.; Sitzmann, H. High-Spin Cyclopentadienyl Complexes: A Single-Molecule Magnet Based on the Aryl-Iron(II) Cyclopentadienyl Type. *Chem. Eur. J.* **2011**, *17*, 4700–4704. [CrossRef]
80. Lin, P.-H.; Smythe, N.C.; Gorelsky, S.J.; Maguire, S.; Henson, N.J.; Korobkov, I.; Scott, B.L.; Gordon, J.C.; Baker, R.T.; Murugesu, M. Importance of Out-of-state Spin–orbit Coupling for Slow Magnetic Relaxation in Mononuclear Feii Complexes. *J. Am. Chem. Soc.* **2011**, *133*, 15806–15809. [CrossRef] [PubMed]
81. Zadrozny, J.M.; Xiao, D.J.; Atanasov, M.; Long, G.J.; Grandjean, F.; Neese, F.; Long, J.R. Magnetic Blocking in a Linear Iron(i) Complex. *Nature Chem.* **2013**, *5*, 577–581. [CrossRef]
82. Eichhofer, A.; Lan, Y.; Mereacre, V.; Bodenstein, T.; Weigend, F. Slow Magnetic Relaxation in Trigonal-planar Mononuclear Fe(ii) and Co(ii) Bis(trimethylsilyl)amido Complexes—A Comparative Study. *Inorg. Chem.* **2014**, *55*, 1962–1974. [CrossRef]
83. Zadrozny, J.M.; Long, J.R. Slow Magnetic Relaxation at Zero Field in the Tetrahedral Complex $[Co(SPh)4]^{2-}$. *J. Am. Chem. Soc.* **2011**, *133*, 20732–20734. [CrossRef]
84. Zadrozny, J.M.; Liu, J.; Piro, N.A.; Chang, C.J.; Hill, S.; Long, J.R. Slow Magnetic Relaxation in a Pseudotetrahedral Cobalt(ii) Complex with Easy-plane Anisotropy. *Chem. Commun.* **2012**, *48*, 3927–3929. [CrossRef] [PubMed]
85. Yang, F.; Zhou, Q.; Zhang, Y.; Zeng, G.; Li, G.; Shi, Z.; Wang, B.; Feng, S. Inspiration from Old Molecules: Field-induced Slow Magnetic Relaxation in Three Air-stable Tetrahedral Cobalt(ii) Compounds. *Chem. Commun.* **2013**, *49*, 5289–5291. [CrossRef] [PubMed]
86. Boča, R.; Miklovič, J.; Titiš, J. Simple Mononuclear Cobalt(ii) Complex: A Single-molecule Magnet Showing Two Slow Relaxation Processes. *Inorg. Chem.* **2014**, *53*, 2367–2369. [CrossRef] [PubMed]
87. Vallejo, J.; Castro, I.; Ruiz-Garcia, J.; Cano, J.; Julve, M.; Lloret, F.; De Munno, G.; Wernsdorfer, W.; Pardo, E. Field-induced Slow Magnetic Relaxation in a Six-coordinate Mononuclear Cobalt(ii) Complex with a Positive Anisotropy. *J. Am. Chem. Soc.* **2012**, *134*, 15704–15707. [CrossRef]
88. Colacio, E.; Ruiz, K.; Ruiz, E.; Cremades, E.; Krzystek, J.; Carretta, S.; Cano, J.; Guidi, T.; Wernsdorfer, W.; Brechin, E.K. Slow Magnetic Relaxation in a Coii–yiii Single-ion Magnet with Positive Axial Zero-field Splitting. *Angew. Chem. Int. Ed.* **2013**, *125*, 9300–9304. [CrossRef]
89. Zhu, Y.-Y.; Cui, C.; Zhang, Y.-Q.; Jia, J.-H.; Guo, X.; Gao, C.; Qian, K.; Jiang, S.-D.; Wang, B.-W.; Wang, Z.-M. Zero-field slow magnetic relaxation from single Co(ii) ion: A transition metal single-molecule magnet with high anisotropy barrier. *Chem. Sci.* **2013**, *4*, 1802–1806. [CrossRef]
90. Habib, F.; Luca, O.R.; Vieru, V.; Shiddiq, M.; Korobkov, I.; Gorelsky, S.I.; Takase, M.K.; Chibotaru, L.F.; Hill, S.; Crabtree, R.H.; et al. Influence of the Ligand Field on Slow Magnetization Relaxation versus Spin Crossover in Mononuclear Cobalt Complexes. *Angew. Chem. Int. Ed.* **2013**, *52*, 11290–11293. [CrossRef]
91. van Stapele, R.P.; Beljers, H.G.; Bongers, P.F.; Zijlstra, H. Ground State of Divalent Co Ions in Cs3CoCl5 and Cs3CoBr5. *J. Chem. Phys.* **1966**, *44*, 3719–3725. [CrossRef]
92. Krzystek, J.; Zvyagin, S.A.; Ozarowski, A.; Fiedler, A.T.; Brunold, T.C.; Telser, J. Definitive Spectroscopic Determination of Zero-Field Splitting in High-Spin Cobalt(II). *J. Am. Chem. Soc.* **2004**, *126*, 2148–2155. [CrossRef]
93. Kulik, H.J. Making machine learning a useful tool in the accelerated discovery of transition metal complexes. *WIREs Comput. Mol. Sci.* **2019**, *10*, e1439.
94. Alvarez, S.; Llunell, M. Continuous symmetry measures of penta-coordinate molecules: Berry and non-Berry distortions of the trigonal bipyramid. *J. Chem. Soc. Dalton Trans.* **2000**, 3288–3303. [CrossRef]

Disclaimer/Publisher's Note: The statements, opinions and data contained in all publications are solely those of the individual author(s) and contributor(s) and not of MDPI and/or the editor(s). MDPI and/or the editor(s) disclaim responsibility for any injury to people or property resulting from any ideas, methods, instructions or products referred to in the content.